REPORT DOCUMENTATION PAGE

Form Approved
OMB No. 0704-0188

1. AGENCY USE ONLY (*Leave Blank*)	2. REPORT DATE	3. REPORT TYPE AND DATES COVERED
	September 21, 1995	Final Report 4/95 - 9/95

4. TITLE AND SUBTITLE
Feasibility Study on a ^{252}Cf Plasma Desorption Imaging Mass Detector.

5. FUNDING NUMBERS
G W81EWF-5031-0261
C DACA39-95-R-0041

Client Code: C000396

6. AUTHOR(S)
Alan M. Levine, Ph.D.
Nicholas W. M. Ritchie, Ph.D.

7. PERFORMING ORGANIZATION NAME(S) AND ADDRESS(ES)
RJ Lee Group, Incorporated
350 Hochberg Road
Monroeville, PA 15146

8. PERFORMING ORGANIZATION REPORT NUMBER
GAH503433 Final Report

9. SPONSORING/MONITORING AGENCY NAME(S) AND ADDRESS(ES)
U. S. Army Engr. CEWS-CT
3909 Halls Ferry Road
Vicksburg, MS 39180-6199

10. SPONSORING/MONITORING AGENCY REPORT NUMBER
Not Known

11. SUPPLEMENTARY NOTES
None

12a. DISTRIBUTION/AVAILABILITY STATEMENT
None

12b. DISTRIBUTION CODE
None

13. ABSTRACT (*Maximum 200 words*)

The overall objective of the Phase I work was to evaluate certain key technical aspects of a proposed Imaging Mass Detector. The proposed instrument consists of a time-of-flight fission fragment plasma desorption mass spectrometer with a novel imaging system for locating the position on the specimen from which molecules are desorbed. Mass Spectrometers which utilize fission fragments to plasma desorb molecular ions from samples have been characterized in the scientific literature and did not require further development. The unique untested principle of the proposed system was that of tracking the fission fragments and combining the mass and spatial information to develop mass images of specimens. The primary task of this Phase I program was, therefore, to identify, test, and evaluate the most suitable spatial detector technology. The main results of the investigation has been to demonstration that such a design is feasible and to provide a layout of a plausible system.

14. SUBJECT TERMS			15. NUMBER OF PAGES
Imaging	^{252}Cf	Californium	
Plasma Desorption	Mass Spectrometer	Fission Fragment	16. PRICE CODE

17. SECURITY CLASSIFICATION OF REPORT	18. SECURITY CLASSIFICATION OF THIS PAGE	19. SECURITY CLASSIFICATION OF ABSTRACT	20. LIMITATION OF ABSTRACT
			UL

Table of Contents

I Executive Summary

1.0 Introduction • Project Objectives and Results

The overall objective of the Phase I work was to evaluate certain key technical aspects of a proposed Imaging Mass Detector (IMD). This was achieved via a combination of literature review, "paper" modeling, and computer-aided design (CAD) with limited bench level experiments to characterize significant untested principles. The main results of this exercise have been to provide a layout of a plausible design and to demonstration that such a design is feasible.

The proposed instrument consists of a time-of-flight (TOF) fission fragment plasma desorption mass spectrometer with a novel imaging system for locating the position on the specimen from which molecules are desorbed. Mass spectrometers which utilize fission fragments to plasma desorb molecular ions from samples have been developed by various industrial and academic institutions [see references in Appendix A] and at least one commercial instrument has been marketed [Bio-Ion, Sweden]. The unique untested principle of the proposed system was that of tracking the fission fragments and combining the mass and spatial information to develop mass images of specimens. The main task of the Phase I program was, therefore, to identify, test, and evaluate the most suitable spatial detector technology.

The outcome of the Phase I development program encompasses the following main results:

1. The feasibility of the proposed imaging concept has been demonstrated and its limitations have been evaluated. Based on this work, the designed system is expected to provide mass images of specimens with a spatial resolution of 1 μm to 50 μm for masses as high as 30,000 amu with mass resolution up to 1 part in a thousand. Imaging times are expected to range from 10 to 60 minutes.

2. The simultaneous detection of x-rays from specimens has been shown to be useful only as a composite analysis over the entire specimen.

3. A first-order engineering design for an IMD system has been provided, which establishes key geometric and electronic relationships and permits projection of the attributes of a prototype instrument.

4. The safety issues surrounding the use of a radioactive source have been addressed with a simple design which contains and monitors the fission source and only allows its introduction into the system if no leakage is detected. This should minimize concerns about the radioactive hazards of ^{252}Cf.

2.0 Brief Summary of the Designed IMD System

The Phase I work has resulted in the design of two instrument configurations. One, referred to as the *transmission system*, is better suited for samples which can be readily prepared to thicknesses of <<10μm. The other, referred to as the *telescopic system*, does not require as extensive sample preparation and can be used to study thicker samples.

Figure 8 is a scaled drawing of the transmission system. This instrument is configured with a single scintillant film on which an ultra-thin sample is mounted. After a fission fragment strikes the sample and desorbs ions, it passes through the sample, strikes the scintillator, and is imaged with an intensified charge coupled device (ICCD) camera. In addition to imaging the light output from fission fragments, detection of penetrating α -particles from the ^{252}Cf source, can provide a density map of the sample, thus providing complimentary information to the mass image. Since the samples must be ultra-thin, considerable sample preparation is required. Satisfactory samples could be prepared by standard techniques such as microtoming or grinding. While this system could be used for soil samples, we feel it would be more appropriate for studying biological samples.

Figure 7 is a scaled drawing of a telescopic instrument. This instrument tracks the trajectory of fission fragments before they strike the specimen. This instrument configuration uses one scintillator film between the source and sample to track the desorbing fission fragment. Each fission event generates two fragment moving in opposite directions. Another scintillator film behind the source locates the partner (*recoil*) fragment. The trajectory of the desorption fragment is determined from these two measurements and is extrapolate to the location on the specimen where the fission fragment strikes, and from which the ions are desorbed. The scintillator films must be thin (1μm to 5μm) so fragments can pass though them with minimal loss of kinetic energy (<10%). Thin scintillator films were produced and will be tested as part of the Phase II work. An ICCD camera is required to monitor each scintillator, which adds the cost of an extra ICCD camera to this configuration compared to the transmission instrument. Since the fission fragments do not have to pass through the specimen, the thickness of the specimen is irrelevant and little sample preparation is required. Since we feel this design has greater utility, we have focused our efforts on its development.

In both systems, desorbed molecular ions are accelerated in an electric field into a time-of-flight mass spectrometer for determination of mass. A mass image is developed by associating mass data from the mass spectrometer with position data from the fission fragment imaging system.

3.0 Work Performed in Phase I and Summary of Results

The major system components of the IMD are a TOF mass spectrometer, a fission fragment source, an imaging system, and a data management system. The TOF and the fission fragment source are off-the-shelf components. The telescopic imaging system is composed of an arrangement of two spatial detectors, each consisting of a thin film scintillator, a lens system, and an ICCD camera. Data management software will be selected or developed, as necessary, during the Phase II and Phase III programs.

The tasks requiring software are listed below:

1. Camera system data acquisition, discrimination and analysis
2. Trajectory determination
3. TOF system data acquisition and analysis, including start and stop signal, reflectron fragment monitoring
4. Mass spectra database and sample comparison
5. Mass/location coordination, analysis, and imaging
6. Source monitoring acquisition and safety control

The system components were evaluated through literature reviews, theoretical evaluations, evaluation of commercially available components, and, when necessary, through data collected from limited bench tests. The following is a brief summary of the results of this work. Details are provided in the attached appendices.

3.1 Source, Sample, and Start Detector Layout

The ^{252}Cf source is an off-the-shelf item [Isotope Product Laboratories]. It is located above the sample in direct line-of-sight of the sample and off of the symmetry axis of the TOF (see Figure 8). The available source is sufficiently thin to allow both fission fragments to escape with minimal energy loss. The system designed in this program will include a novel containment system for the source. The containment system retracts the source into a locked sealed safe while not in use. For safety, the source container has a monitoring sensor within it and will not unlock if any leakage is detected. The source safe can be removed from the system and shipped for repair without loss of containment.

The sample stage was designed with the following features:

1. Sample introduction with minimal disruption to vacuum
2. Electrical isolation
3. Flat and large to prevent perturbation of electric field
4. Allow for liquid nitrogen cooling to decrease the vapor pressure of volatile samples

Figure 1. Source, Sample, and Start Detector Layout.

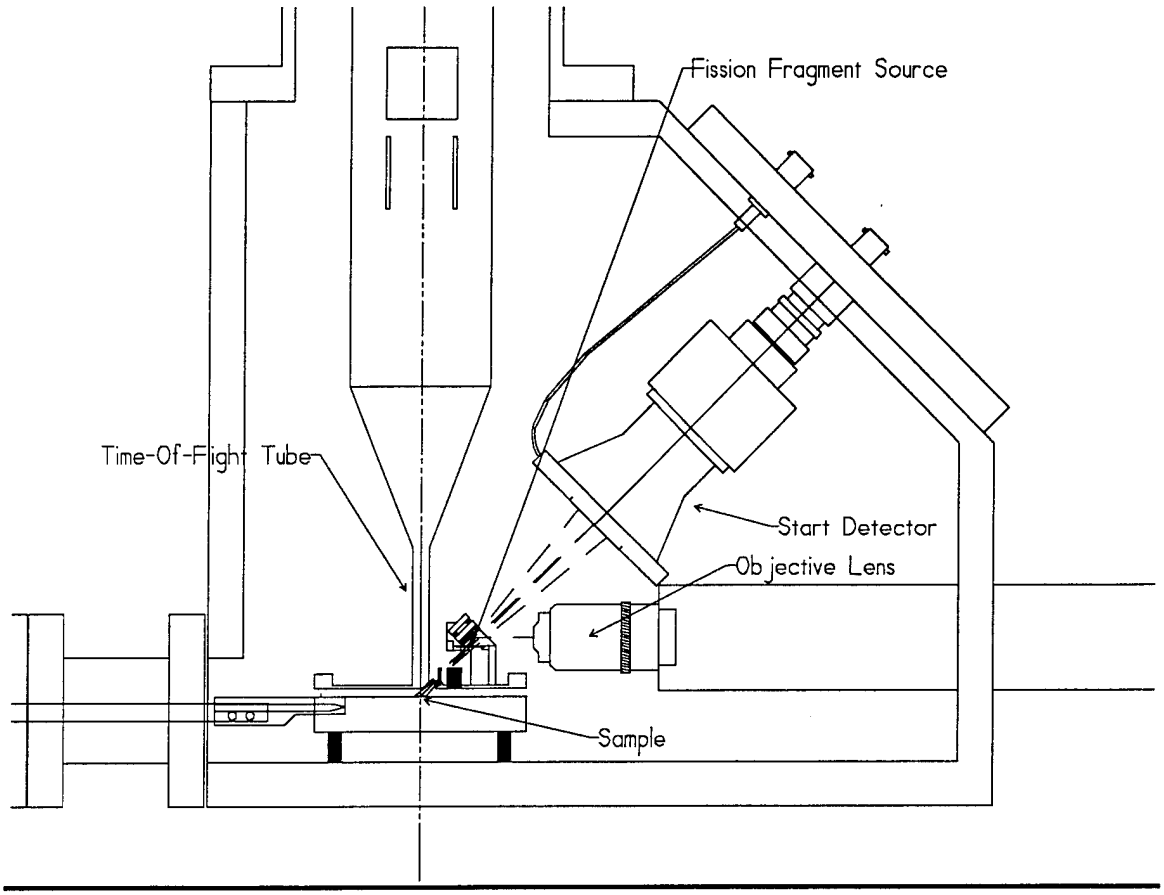

The TOF start signal will be obtained from recoil fragments striking a microchannel plate. The geometric relationship of these components is shown in Figure 1. Details of these components are reviewed in Appendix F.

3.2 Evaluation of Time-of-Flight Mass Spectrometers

As part of the Phase I work, we identified and evaluated several TOF systems which apply modern technologies and could readily be adapted to this instrument. The results of our evaluation of TOF systems is reviewed in Appendices A and B. Based on this evaluation, we found that state-of-the-art mass spectrometers are available which could be readily adapted to this application. We chose to incorporate a commercial system from Comstock of Oak Ridge, Tennessee for the Phase I design rather than develop our own TOF. This system includes a two-meter folded flight tube with a Mamyrin reflectron. In addition to decreasing the dimensions of the TOF, the reflectron increases the mass resolution by correcting for variations in initial kinetic energies of the ions as they enter the system. A drawing of the Comstock system is shown in Figure 3.

3.3 Evaluation of Spatial Detectors

A key part of the imaging system are detectors which will be used to determine the spatial position of fission fragments. The fission fragments must not lose a significant portion of their energy as they passes through the spatial detector. We searched the technical and commercial products literature and were unable to identify any applicable detectors. Therefore, we designed our own novel detector. We identified two detector designs, scintillator and impulse, which we felt would be applicable to this instrument. Briefly, the scintillator system uses ICCD cameras to locate light flashes produced when fission fragments pass through scintillator films. The impact detector analyzes acoustic compression waves produced by fission fragments as they impact a thin metal foil (see Appendix H. Details of various aspects of this evaluation are summarized in Appendices G through N. After initial bench tests to investigate design parameters of the impulse, or acoustic, detector we determined that it would be extremely sensitive to vibrations and would require sophisticated mechanical isolation. Since the scintillator design is robust, we concentrated on testing this design for the prototype system.

Various scintillators were evaluated through a literature review and bench level tests to characterize their interactions with energetic ions. From these evaluations, ZnS(Ag) was selected based on light output and ease of handling. ZnS(Ag) is a polycrystalline powder, which can be embedded in a resin to form a durable membrane. Using microtoming techniques these membranes can be made as thin as 1 μm. It remains for Phase II to determine the optimal grain size and film thickness for fission fragment imaging.

The spatial resolution of various scintillators was evaluated at the bench with photographic film. Due to the availability of a polonium source, which is an α emitter, the initial testing was performed with α-particles. The photographic test considered the shadow of a mask placed directly on the scintillator surface. The mask blocked the α-particles from some of the scintillator. By carefully examining the sharpness of the transition between dark and light where the α-particles were or were not blocked we could estimate the resolution. These tests demonstrated that the ZnS(Ag) scintillator was capable of resolutions better than 30 μm. These tests were limited by the grain size of the photographic film and the available optics.

To verify that we could image single scintillation events, we performed a series of tests using an ICCD camera, which was on loan from XYBION of California. Theoretical considerations and details of this investigation are covered in Appendix L. These tests demonstrated that single scintillations can be imaged and digitized using currently available instrumentation. Using the results from these tests we developed the layout of the proposed system shown in Figure 4.

Since californium emits α-particles as well as fission fragments, it was important to show that the proposed detector would distinguish between these two particle types. This was tested by N. Ritchie, W. Ulbricht, and W. Pitts using both α-particles and fission fragments at Greenspan Incorporated in Houston, Texas. The details of these tests are described in Appendix N. While these tests answered some of our questions, some questions remained unanswered. We demonstrated that >25% of fission fragments produce more scintillator output than the brightest α-particles. This value may be artifactually low due to limitations in the experimental design. While 25% is sufficient to produce a prototype instrument, results indicate that further testing and optimization of the scintillators with ^{252}Cf fission fragments should be pursued as part of the Phase II program.

3.4 Evaluation of Imaging Methodology

A problem was discovered with the telescopic concept presented in the Phase I proposal. The Phase I proposal assumed that the pair of fission fragments produced in a fission event follow anti-parallel trajectories. However, due to neutrons emitted immediately following the fission event, the fission fragments can deviate by as much as 0.6° from antiparallel trajectories. See Appendix D for a detailed discussion of the effects of spontaneously generated neutrons on fission fragment trajectories. Although, the variations in path angle are small, the deviations cause significant errors when projecting the location of the desorption on the specimen. Since the spatial error associated with the emission of neutrons is small when measured close to the source, one detector can be located immediately behind the source to locate the fission event. However, the second detector in the telescope must be located between the source and the sample to locate the desorption fragment. This poses the limitation that the scintillator plate must be thin (on the order of 1μm to 5μm) in order not to absorb significant amounts of energy from the fission fragments during their passage. The recommended thickness is based on both theoretical calculations and literature reviews outlined in Appendix E. Refer to Appendix C for a summary of the properties of fission fragments. Scintillators and imaging methodologies are reviewed in Appendix B. This arrangement is outlined in Figure 2 and details are summarized in Appendix I.

3.5 Evaluation of X-Ray Emission

Tests, presented in Appendix O, showed the emission of x-rays generated by a large flux of α-particles. Although x-rays were detected, the level was low and would only be useful if they were accumulated over the entire sampling time. This test does not directly address the emission of x-rays produced during the desorption by fission fragments, it indicates that levels would probably be low and would only be useful as a bulk analysis.

Figure 2. Layout of Telescopic System.

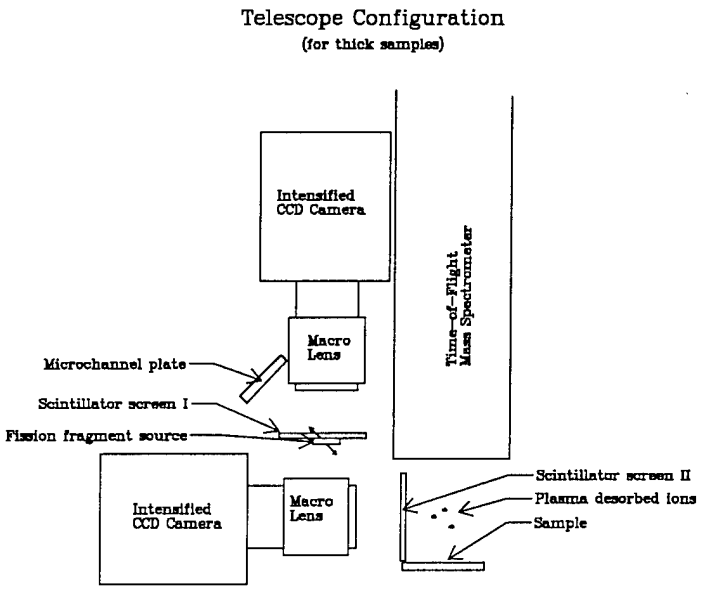

Figure 3. Time-of-Flight Configuration.

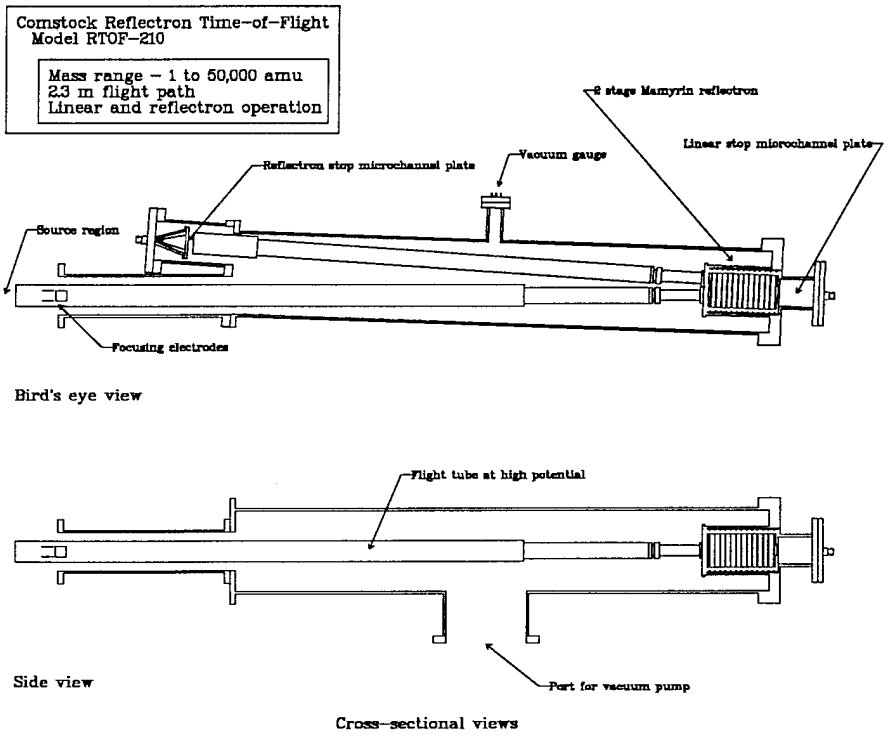

Figure 4 - Spatial Detector Layout

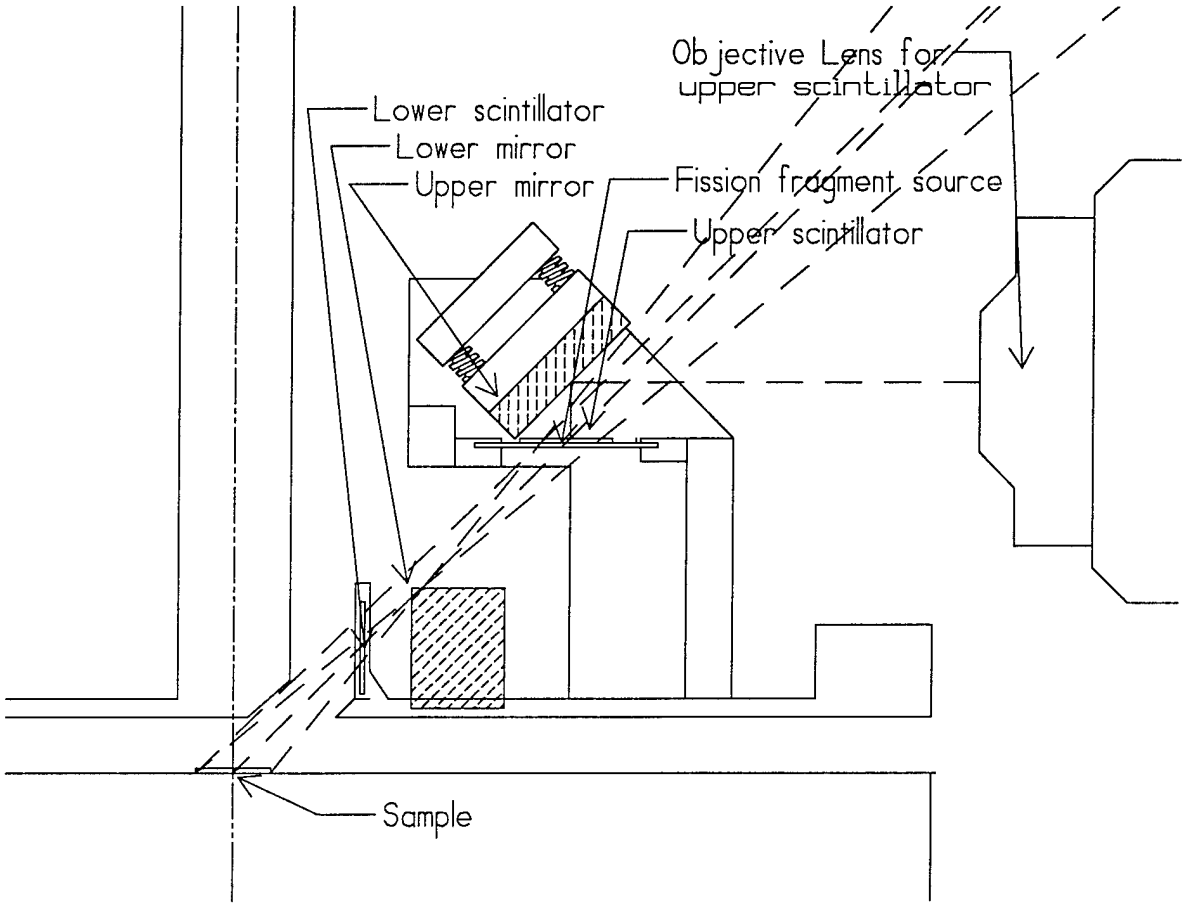

3.6 Scaled Drawings of IMD Designs

Two instrument designs are presented, transmission and telescopic, based on the Phase I study. These are outlined schematically in the flow charts in Figures 5 and 6. Scaled layouts of these instruments are provided in the CAD drawings in Figures 7 and 8.

Figure 5. Telescopic Instrument To Be Used With Thick Samples

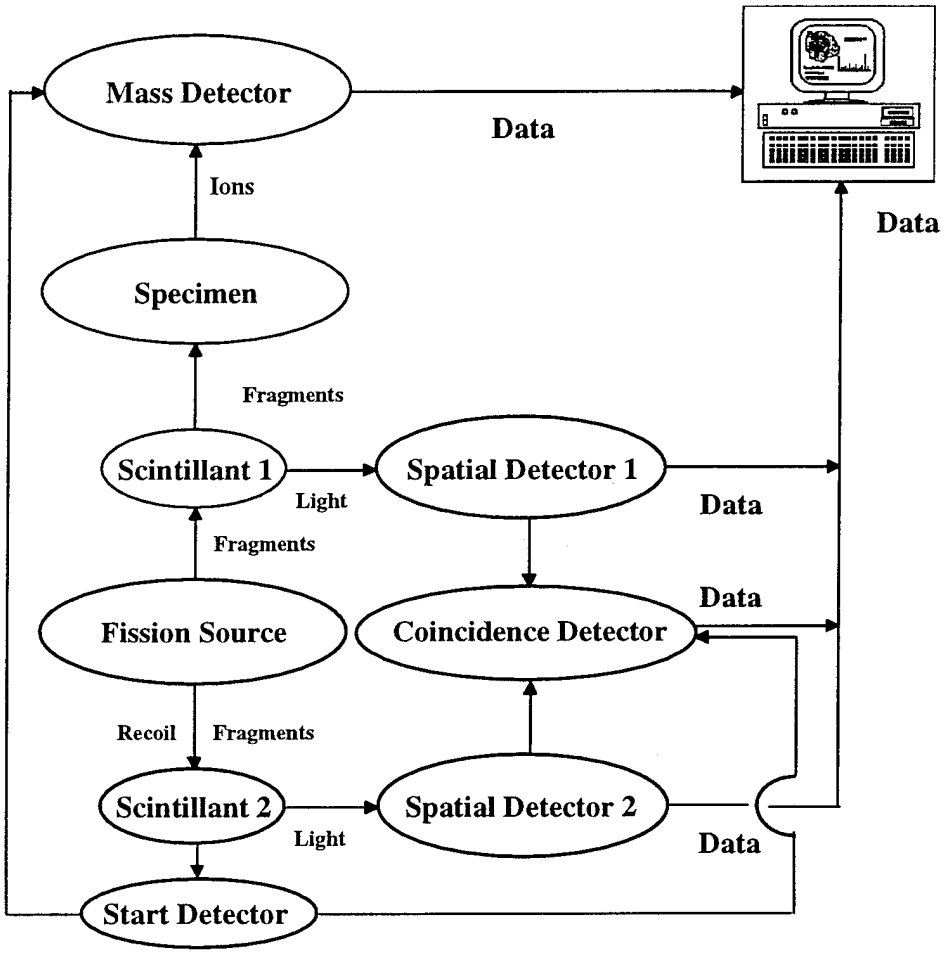

Figure 6. Transmission Instrument To Be Used With Thin Samples

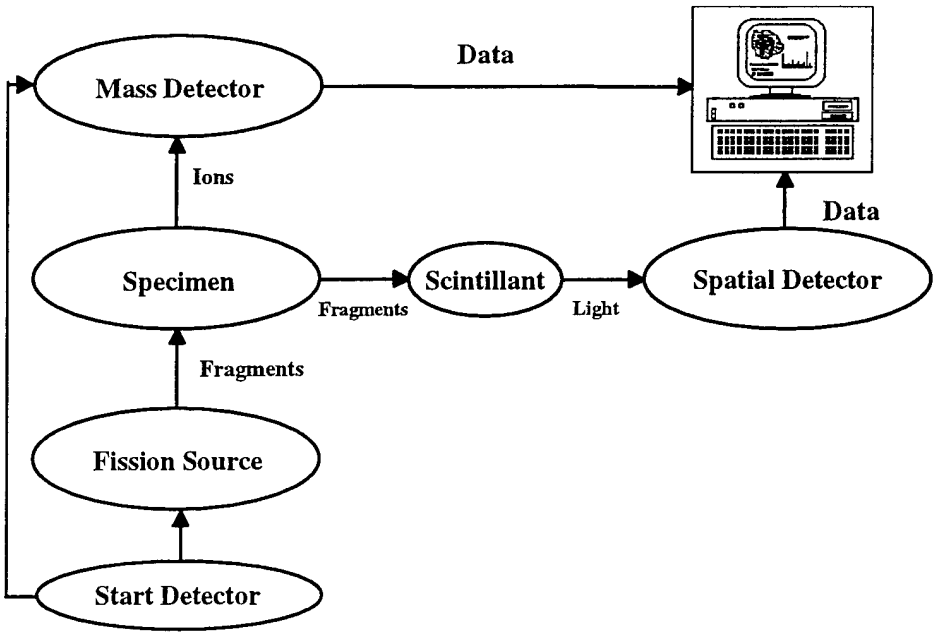

Figure 7. Scale Layout of Telescopic Instrument.

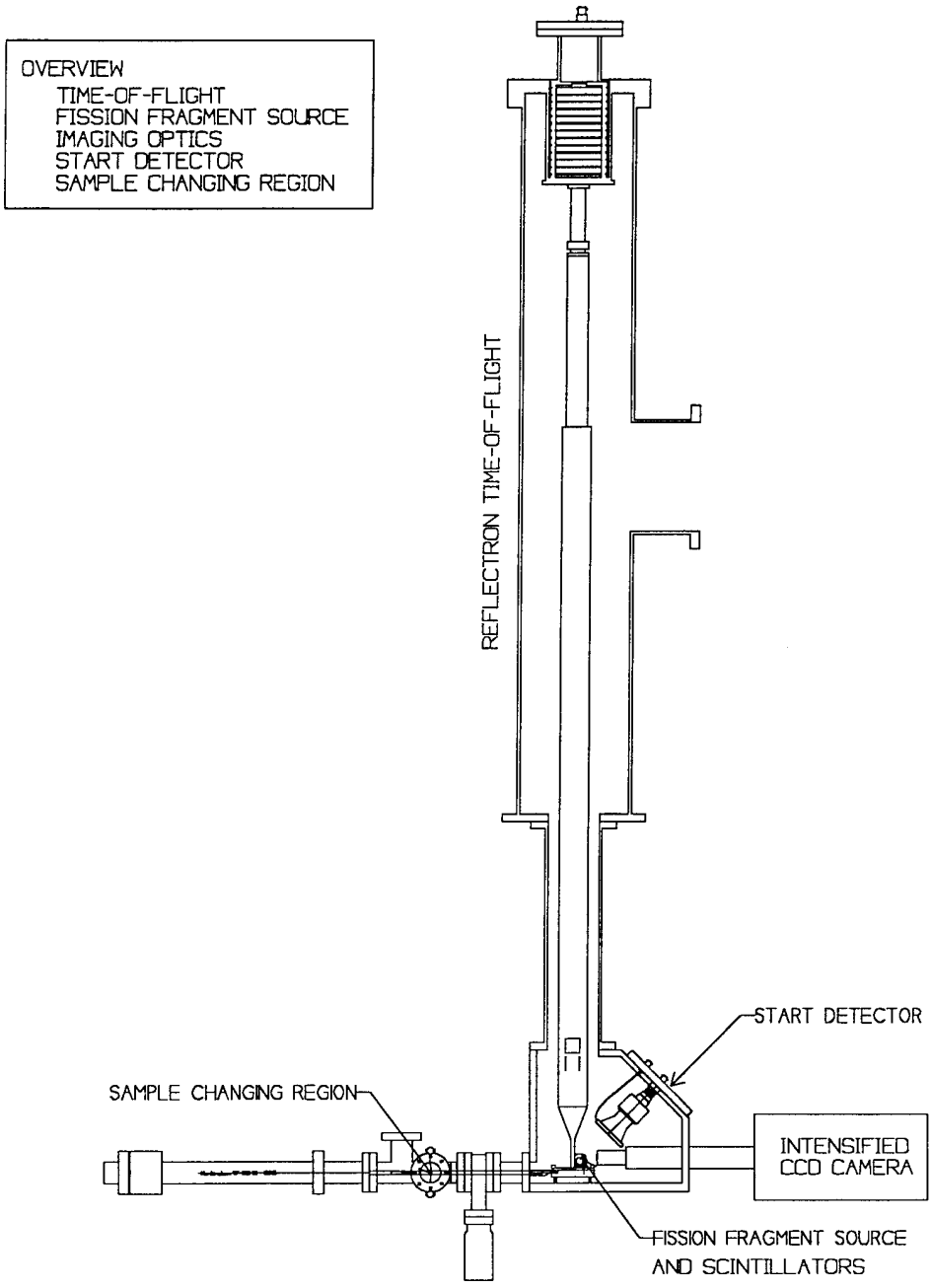

Figure 8. Dimensioned Layout of Transmission Instrument.

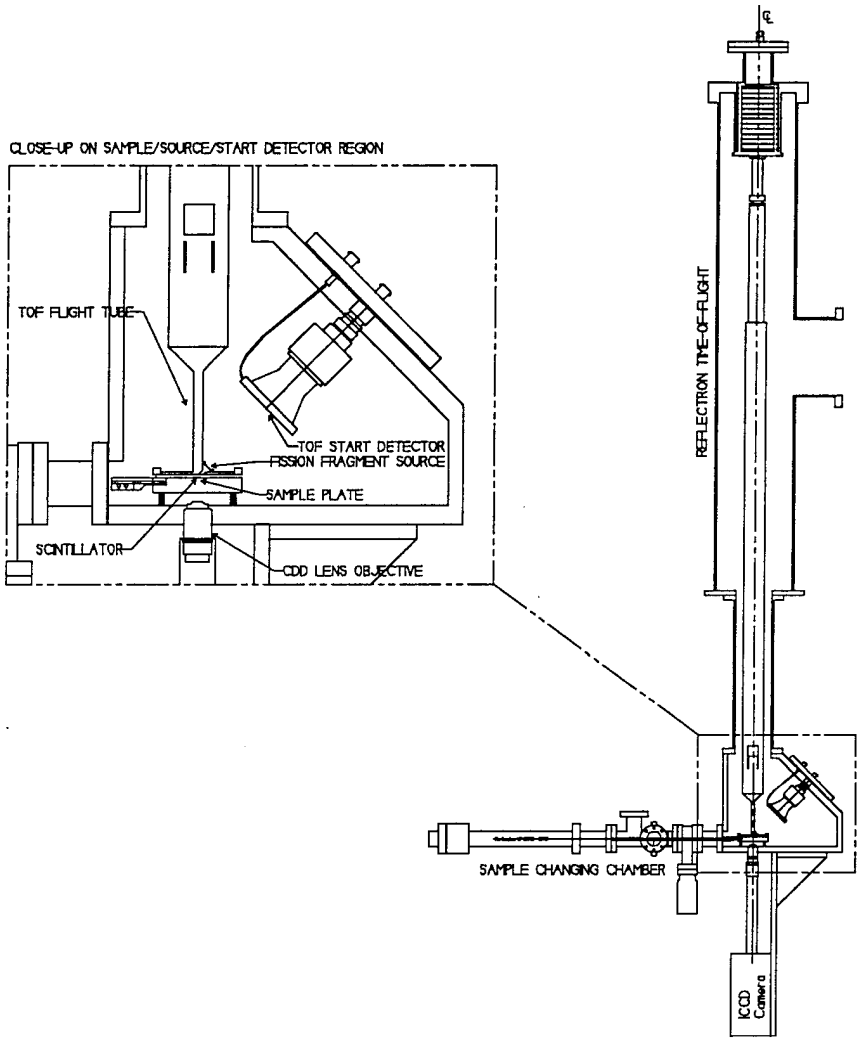

3.7 Instrument Specification

Estimated Prototype System Materials Costs: $154,000

Material	Estimated Cost
Source	$2,500
TOF	$26,000
ICCD's	$30,000
Custom Lens Systems	$15,000
Computer	$3,000
Computer Interfaces	$2,500
Software	$1,000
Vacuum System	$14,000
Electronics	$28,000
Machining	$12,000
Miscellaneous Supplies	$20,000
Total	$154,000

Mass Resolution of TOF Spectrometer:	1 part in 1000 or better
Mass Range:	0 through 30,000+ amu
Achievable Spatial Resolution:	1μm to 30μm
Source Type:	^{252}Cf
Source Size:	10 μCi
Power:	120 VAC
Weight:	approx. 400 lbs
Dimensions:	4'x4' footprint; 8' height

Data Collection System

Hardware:	Pentium/100 MHz
	16 MB RAM
	1.2 GB Hard Drive
Acquisition Boards:	ICCD's, TOF, Other Activities
Software:	DOS/Windows/Acquisition/Data Base
	Imaging/Mass Spectra

II Appendices

Appendix A - Overview of Plasma Desorption Mass Spectrometry (PDMS)

Plasma desorption mass spectrometry (PDMS) uses energetic fission fragments to volatilize and ionize a solid sample. The mass of the volatilize and ionized molecule is measured in a time-of-flight mass spectrometer. The PDMS technique was developed in 1974 by D. F. Torgerson, R. P. Skowronski and R. D. Macfarlane[1]. An excellent introduction to PDMS is available in R. D. Macfarlane and D. F. Torgerson's Science article[2].

PDMS uses the energetic particles (fission fragments) formed when a heavy atom fissions into two lighter ions to plasma desorb molecular unfragmented ions (or almost unfragmented) from the surface of a sample. A source of fissile material (typically ^{252}Cf) is situated near the surface of a sample of unknown molecular composition. The nucleus of ^{252}Cf is inherently unstable and after a period of time spontaneously breaks up into two smaller nuclei. These nuclei are called fission fragments and for ^{252}Cf are approximately of masses 106 and 142 amu. See Appendix C for more details on ^{252}Cf and fission fragments. The ^{252}Cf nucleus releases about 180 MeV in the fission process. Most of this energy is becomes kinetic energy in the fission fragments. On average, the lighter fragment gets 103 MeV and the heavier fragment gets 79 MeV. In addition, the fission fragments tend to be highly ionized (~20e^-). Some of the fission events will produce a fission fragment with a trajectory towards the surface of the molecular sample. This fragment will be referred to as the *desorption fragment.* Because of conservation of momentum, the other fission fragment from the fission event will travel in almost exactly the opposite direction. This fragment will be referred to as the *recoil fragment.* Since the recoil fragment occurs simultaneous to the desorption fragments, the recoil fragment is often used for the start signal for the time-of-flight.

When the desorption fragment strikes the sample surface it heats a localized region of ~5000 Å[2] boiling off ions in the process[3]. Typically these ions have temperatures of approximately 10^4 K[1]. Because the heating occurs so quickly, the molecules tend not to absorb the energy into vibrational modes and are desorbed whole or nearly whole. The desorption of unfragmented molecular ions is referred to as *soft desorption.*

The mass of a desorbed molecular ion is measured in a time-of-flight mass spectrometer (TOF-MS). A static electric field accelerates the ion to a kinetic energy which depends on the ionization potential of the molecule but is independent of mass. The trajectory of the molecule over a specific distance is timed and since the kinetic energy of the molecule is known (assuming a singly ionized molecule), the mass is proportional to the square of the time-of-flight.

---

1 D. F. Torgerson, R. P. Skowronski and R. D. Macfarlane Biochem. Biophys. Res. Commun. 60, 616 (1974)

2 R. D. Macfarlane and D. F. Torgerson, Science **191**, 920 (1976).

3 A. Chatterjee, H. D. Maccabee, C.A. Tobias, Radiol. Res. **54**, 479 (1973)

PDMS has proven itself as an important technique for the study of large involatile biomolecules[4]. It has also been demonstrated as a powerful technique for studying large inorganic clusters[5] by McNeal. William Ulbricht has also demonstrated using the PDMS technique with U_3O_8 to do isotopic studies[6].

We have prepared soil samples with various different lead-based molecules to demonstrate the applicability of PDMS to the study of heavy metal ions.

The Army Corps of Engineers solicited this SBIR research for the purpose of developing an instrument to speciate metal containing compounds in soil samples. To test PDMS on a metal-containing compound in a soil matrix, we spiked a soil sample with approximatelly 200 ppm of lead naphthenate, a common paint ingredient, and had it analyzed on a Bio-Ion system by a collegue. The chemical structure of lead naphthenate is as follows:

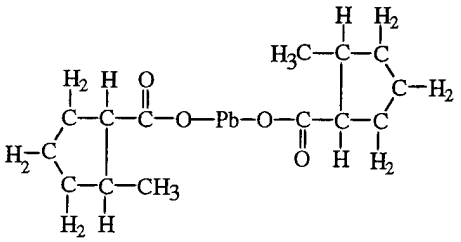

Lead Naphthenate
Mw = 461.53

The sample was extracted with ethyl acetate, the extract was added to water, and then analyzed. The results of this analysis showed a mass peak where this compound would be expected. This spectrum was weak due to the inclusion of the extraction step.

Additional References

C. J. McNeal, R. D. Macfarlane, E. L. Thurston, "Electrospray method for PDMS studies of Involatile Molecules", Anal. Chem. 51, no. 12, p. 2036-2039 (1979)

P. A. van Veelen, U. R. Tjaden, J. van der Greef, "Internal Energy content of ions in 252-Cf plasma desorption mass spectroscopy" Int. J. Mass Spect. and Ion Proc. 110 (1991)

G. Allmaier, E. R. Schmid, "Californium-252 plasma desorption mass spectrometry as a tool for studies of metallocenes", Int. J. Mass Spect. & Ion Proc. vol.126 p.211-20 (1983)

I. Kamensky, A. G. Craig, " ^{252}Cf plasma desorption mass spectrometry: recent advances and applications", Analytical Instrumentation vol.16, no.1 p.71-91 (1987)

---

4 R. B. Cody, Jr., J. A. Kinsinger, S. Ghaderi, I. J. Amster, F. W. McLafferty, and C. E. Brown, Anal. Chim. Acta., 178 (1985) 43.] [D. A. Laude, Jr., C. L. Johlman, R. S. Brown, D. A. Weil and C. L. Wilkins, Mass Spectrom. Rev., 5 (1986) 107.

5 C. J. McNeal, J. M. Hughes, G. J. Lewis, and L. F. Dahl, J. Am. Chem. Soc. 113 (1991) 371

6 W. H. Ulbricht, Jr., Proceedings of the 25th Conference of Analytical Chemistry in Energy Technology, (1981)

R. D. Macfarlane, J. C. Hill, D. L. Jacobs, "A new californium-252 plasma desorption time-of-flight mass spectrometer for high-mass studies", Analytical Instrumentation vol.16, no.1 p.51-69 (1987)

R. D. Macfarlane, "Californium-252 plasma desorption mass spectrometry", Analytical Chemistry vol.55, no.12 p.1247A-64 (1983)

W. Tuszynski, R. Angermann, J. O. Metzger, R. Woisch," Production of polyatomic ions by /sup 252/Cf-fission fragments and by short laser pulses", Nucl. Inst. & Meth. in Phys. Res. vol.B88, no.1-2 p.184-90 (1994)

G. Brinkmalm, P. Hakansson, J. Kjellberg, P. Demirev, B. U. R. Sundqvist, W. Ens,"A plasma desorption time-of-flight mass spectrometer with a single-stage ion mirror: improved resolution and calibration procedure", International Journal of Mass Spectrometry and Ion Processes vol.114, no.3 p.183-207 (1992)

P. W. Geno, R. D. Macfarlane, "^{252}Cf plasma desorption mass spectrometry using a Mamyrin reflectron in a low voltage regime", International Journal of Mass Spectrometry and Ion Processes vol.77, no.1 p.75-94 (1987)

P. W. Geno, R. D. Macfarlane, "^{252}Cf plasma desorption mass spectrometry at low acceleration voltages using the electrostatic particle guide", International Journal of Mass Spectrometry and Ion Processes vol.74, no.1 p.43-57 (1986)

Appendix B - Evaluation of Time-of-Flight Mass Spectrometer Systems

A time-of-flight spectrometer measures the mass of an ion by accelerating the ion in an electric field and measuring the time it takes for the accelerated ion to fly a certain distance. Rather than reinvent the wheel, for this project we have decided to purchase a commercially available time-of-flight (TOF) mass spectrometer. By purchasing a TOF unit, we are able to take advantage of recent innovations in TOF technology without investing the time and resources necessary to redevelop the technology ourselves. In particular, we will be able to integrate a more sophisticated and higher resolution angular reflectron-type TOF (RTOF) into our instrument.

The reflectron TOF was developed by Mamyrin et al[7]. The RTOF addresses one of the fundamental limitations of TOF spectrometers, that is, the limitation in resolution due todifferent initial ion velocities caused by thermal and other source effects. Particularly in the case of PDMS, the initial thermal velocity of the ions can be relatively large and can pose a significant limitation in the instrument resolution. As in a linear TOF, the ions from the source region are accelerated into the spectrometer by a electrostatic potential difference between the source region and the spectrometer. In a linear TOF, the ions follow this initial trajectory until they strike a stop detector (usually a microchannel plate.) A RTOF is like a linear TOF that has been folded in half by reflecting the ions off an electrostatic ion mirror. In addition to the obvious benefit of reducing the physical size of the apparatus, the electrostatic mirror also compensates for differing initial ion speeds. Faster ions take more time to turn around in the electrostatic mirror and by careful design, the effect of differences in initial velocity can be almost entirely canceled. The exact resolution of the time-of-flight spectrometer depends upon many factors including the timing resolution and the initial thermal velocity spread of the ions.

For our prototype instrument we have chosen the reflectron time-of-flight mass spectrometer from Comstock -- the RTOF-210. Fig. B.1 is a cross-sectional view of a Comstock RTOF-210 reflectron time-of-flight mass spectrometer. The top diagram shows the RTOF-210 from the side and the lower diagram is a view of the instrument rotated by 90° about the symmetry axis. To get a sense of the scale, the flight tube length is 2.3 meters. The source region is to the lower left on each drawing. Comstock does not provide any of the source apparatus, however, the RTOF-210 is designed to easily interface with many different type of sources and Comstock is willing to work with us to make any modifications necessary.

Typically, a vacuum pressure of 10^{-8} Torr or better is required to acquire good time-of-flight spectra. Pressures like this are easy to achieve with a little care. The RTOF-210 is built to standard ultra-high vacuum standards with copper gaskets. The main chamber will be pumped through the 8" diameter vacuum pump port with an ~250 ℓ/s turbo-molecular pump. We have chosen a turbo-molecular pump for its simplicity, robustness, cleanness and low maintenance. In addition to the large pump on the TOF spectrometer, a second smaller pump (60 ℓ/s) will be used to evacuate the sample changing region. This pump will serve multiple purposes. First, it will assist in ensuring that sample outgassing will not negatively effect the overall vacuum pressure. Second, it will allow the user to change samples more quickly by separating the source and TOF regions.

---

7 B. A. Mamyrin, V. I. Karataev, D. V. Shmikk, and V. A. Zagulin, Zh. Eksp. Teor. Fiz. **63,** 1 (1973) p. 82-89

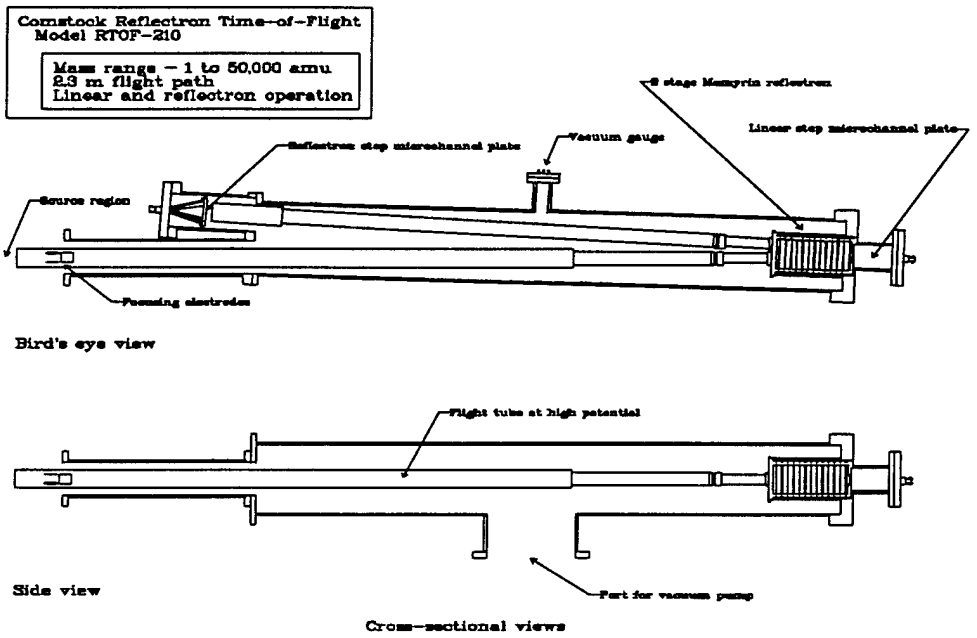

Figure B.1 - Cross-sectional views of the Comstock RTOF-210 reflectron time-of-flight spectrometer.

Appendix C - Properties of ^{252}Cf and Fission Fragments

Fission is the process by which the nucleus of a heavy atom splits into two smaller nuclei and a small number (0-4) of neutrons. When a nucleus fissions, a large quantities (~200 MeV) of energy, which had previously bound the nucleus together, is released as kinetic energy. Most of the binding energy is split between the two product nuclei as kinetic energy. The remainder is carried off by the neutrons. Typically the product nuclei, *fission fragments*, are highly ionized (~20 le-l).

While a number of heavy atoms can be induced with neutrons to fission, very few atoms fission spontaneously. One atom that does fission spontaneously is ^{252}Cf. ^{252}Cf has a spontaneous fission half-life of 85.5 years and an α-particle decay half-life of 2.73 years for an effective half-life of 2.65 years. Even with a half-life of 85.5 years, the average fission rate is $6.2 \cdot 10^5$ /s/μg. Table C.1 summarizes the properties of ^{252}Cf.

---------- from Isotope Product Laboratories product literature ----------	
Spontaneous fission half-life	85.5 years ($2.70 \cdot 10^9$ s)
Average fission rate	$6.2 \cdot 10^5$ /s/μg
Specific activity	536 μCi/μg
α-particle decay half-life	2.73 years ($8.62 \cdot 10^7$ s)
α-particle energy	6.076 MeV and 6.118 MeV
γ emission rate	$18 \cdot 10^7$ photons/s/μg
Neutron properties	
Avg. neutron energy	2.35 MeV
Avg. # of neutrons/fission	3.76
Avg. neutron emission rate	$2.34 \cdot 10^6$ n/s/μg
---------- from Henschel et al. ----------	
Fission fragment properties	
$<m_L>$	106.16 amu
$<m_H>$	142.17 amu
$\sigma(m_L)$	6.60 amu
$\sigma(m_H)$	7.69 amu
$<E_L>$	102.54 MeV
$<E_H>$	78.68 MeV
$\sigma(E_L)$	6.73 MeV
$\sigma(E_H)$	9.15 MeV
$<E_{Tot}>$	181.22 MeV

H. Henschel, A. Kohnle, H. Hipp, G. Gonnenwein, Nucl. Inst. and Meth. in Phys. Res. **190**,.1 (1981) p.125-34

Figure C.1 - Important properties of ^{252}Cf and ^{252}Cf fission fragments

Appendix D - The Effect of Neutron Emission on the Trajectory of Fission Fragments

The imaging mass detector (IMD) in the original Phase I proposal assumed that when the ^{252}Cf fissioned, the resulting two ions would separate along the same line but in opposite directions. One ion would plasma desorb the molecules whose mass would be measured in the time-of-flight mass spectrometer. The other ion, by virtue of its exactly anti-parallel trajectory, would provide position information from which the position of the desorption could be calculated.

If ^{252}Cf behaved like a mass breaking into two parts, this scheme would work well. Conservation of momentum requires that in the rest frame of the original mass, the two particles will separate at 180° relative to one another. However, when Cf fissions it breaks into two ions with unstable nuclei, which almost immediately ($<10^{-14}$ sec) emit between 0 and 4 neutrons[8]. These neutrons are emitted with a Boltzmann distribution of energies with a peak around 1.4 MeV[9].

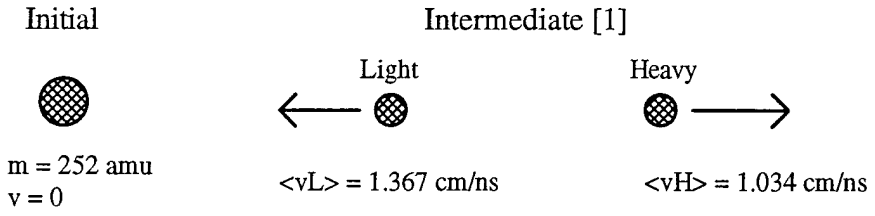

Consider the emission of one neutron from the lighter fragment. Typically, the lighter fragment will have mass of $<m_L> = 106$ amu and the neutron has a mass $m_n = 1$ amu. In center-of-mass (CM) coordinates,

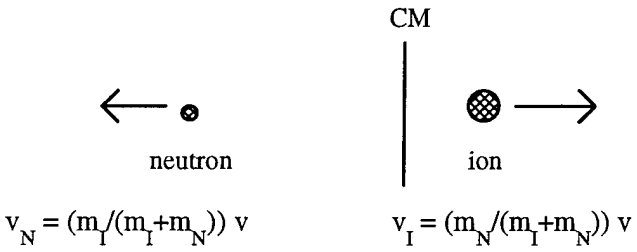

so $v_I = m_N/m_I\ v_N$ and $v_N = (2\ E_N/m_N)^{1/2} = 1.64 \times 10^7$ m/s and $v_I = 1.55 \times 10^5$ m/s $= 1.55 \times 10^{-2}$ cm/ns.

---

8 H. Henschel, A. Kohnle, H. Hipp, G. Gonnenwein, Nuclear Instruments and Methods **190**, (1981) 125-134

9 K. Tanaka, M. Hoshi, S. Sawada, N. Kamada, Int. J. Radiat. Biol. **66**, 4 (1994)

Consider the motion of the CM. The neutron may be emitted in any direction relative to the direction of the propagation of the CM. Label the angle between the direction of propagation of the CM and the direction of the neutron emission with η. The angle of deviation of the ion, θ, will be

$\sin(\theta) = (v_I/\langle v_L \rangle) \sin(\eta) = 1.13 \times 10^{-2} \sin(\eta)$. For $\eta = \pi/2$ (the worst case), $\theta = 1.13 \times 10^{-2}$ or 0.65^{o}.

Given an instrument geometry of 5 cm, this corresponds to a deviation of up to 0.6 mm per neutron per fission fragment. This deviation is many orders of magnitude larger than the intended resolution of our instrument.

These calculations rule out using the recoil fission fragment for position information, unless the recoil fragment is measured very close to the source.

Appendix E - The Interaction of Fission Fragments with Matter

Energy loss through ionization represents the principal mechanism through which energetic ions are slowed down in matter. Fission fragments, which are highly ionized (~20e⁻), tend to interact strongly with matter and are slowed down quite quickly. For comparison, a 100 MeV fission fragment typically has a similar range to a 4 MeV alpha particle despite differences in energy.

For lighter ions, the Bethe-Bloch equation describes quite accurately the rate of the energy loss with distance traveled through the target material, $-dE/dx$[10].

$$S = -\frac{dE}{dx} = \frac{z^2 NZ}{v^2} K\left[\ln(2m_o v^2 / I) - \ln(1-\beta^2) - \beta^2\right]$$

where $K = \frac{e^4}{4\pi\varepsilon_o^2 m_o}$. ze is the ionic charge of the ion where e is the charge of one electron. m_O is the mass of an electron. v is the velocity of the fission fragment and $\beta = v/c$ where c is the speed of light. N and Z are the number of atoms per unit volume and the atomic number of the target material. ε_O is the permittivity of free space.

However, the Bethe-Bloch equation tends to underestimate the range for fission fragments. The Bethe-Bloch equation assumes that the ionization of the fragment is constant. Fission fragments, because of their slower speed and high ionization, tend to pick up electrons more quickly than lighter particles.

While the absolute range of a fission fragment depends upon the density of the target material, the *stopping power* tends to be relatively constant across materials. The stopping power is defined as the energy loss per unit of the product of density times thickness. Examination of the Bethe-Bloch equation suggests that this quantity might be constant and empirically this quantity has been confirmed to be reasonably independent of material.

Batra et al[11] have reported the stopping power for ^{252}Cf fission fragments measured in NE-102, a plastic scintillator material. A copy of their results is plotted in Figure E.1.

Understanding the range of a fission fragment is important regardless of the design of the imaging system. First, for construction of the fission fragment source, the source must be sufficiently thin to allow both fission fragments from a single fission event to escape from opposite sides of the source. Second, the path from the fission fragment source to the sample must be sufficiently unobstructed that the fission fragment can reach the sample with most of its energy remaining. Third, if the fission fragment is to be located using a scintillator below the sample, the sample must be sufficiently thin to allow passage of the fission fragment. To summarize, the Batra and Shotter results suggest that the sample/PSD stopping power must be less than 1 mg/cm^2.

---

10 C. F. G. Delaney and E. C. Finch, Radiation Detectors, Clarendon Press, Oxford (1992)

11 R. K. Batra and A. C. Shotter, Nucl. Inst. and Methods B5 (1984) 14-19

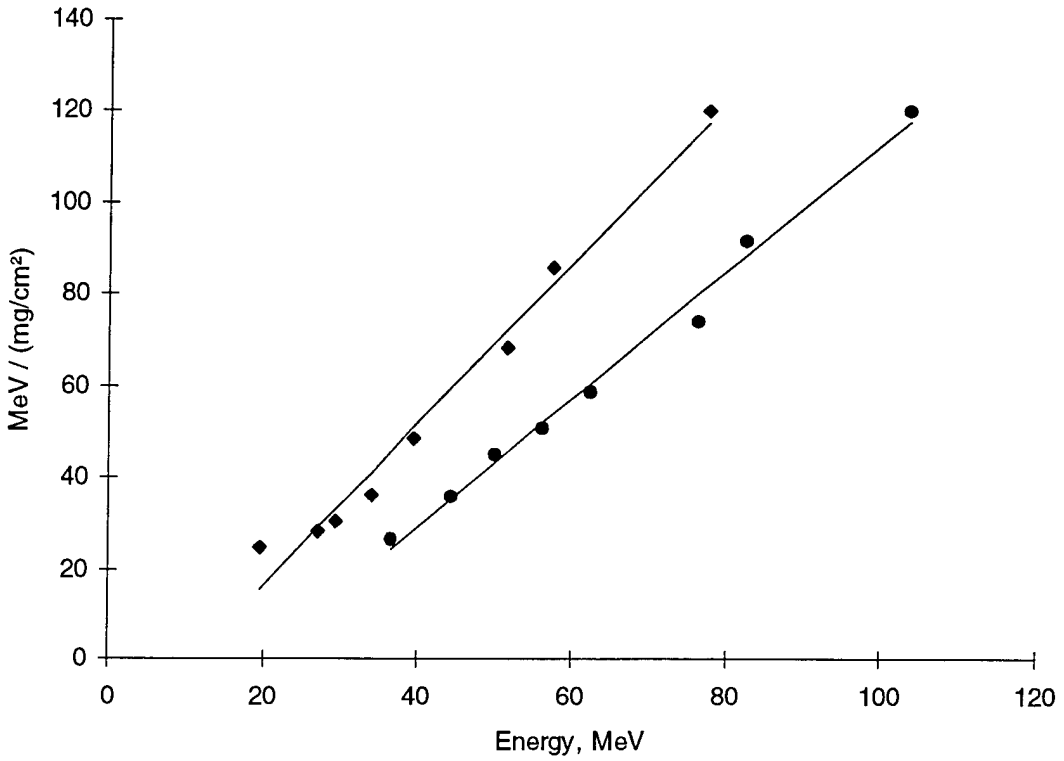

Figure E.1 - Measured stopping powers for the mean light (circles) and heavy (diamonds) fragments vs. energy. Measured in the plastic scintillator NE-102. From R. K. Batra and A. C. Shotter, Nucl. Inst. and Methods B5 (1984) p.14-19. The lines are my best fit lines through the data.

Appendix F - Design details for the Source/ Sample/ Start Detector Layout

The Sample Stage

Overview - The sample stage is designed with the following features.

1. To limit the time required to change samples, the sample stage will be designed to permit changing the sample slide without exposing the TOF system to atmosphere.
2. The sample stage will be electrically isolated from the rest of the system. This allows us to either operate the flight-tube at high potential or at ground.
3. To ensure all ions are accelerated up the axis of the TOF regardless of where on the sample these ions originate, the E-field between the stage and the accelerating grid must be made uniform. This is accomplished by making the sample stage and accelerating grid flat, large and adjustable.
4. The sample stage should allow for the option of liquid nitrogen cooling to decrease the vapor pressure of volatile samples.

Feature 1 is implemented by separating the chamber into two chambers -- the sample changing chamber and the TOF chamber. The two chambers are separated with a gate valve. The sample slide mount can be moved between the chambers with a linear feedthrough. When the sample is in the sample changing chamber the gate valve can be closed isolating the two chambers. The sample changing chamber can be opened to air, the sample changed and the chamber reclosed. A separate vacuum pump will pump down the sample changing chamber. When the sample chamber and the TOF chamber are at similar pressures the gate valve between the two chambers can be opened. By limiting the volume that needs to be pumped, the time required to pump down will be held down to a minimum. The Phase I design and the Phase II prototype will be designed with this feature, however, we expect the sample changing chamber will be implemented in Phase III.

Feature 2 is implemented by isolating the sample stage from the chamber with vacuum compatible machinable ceramics. The mounting legs of the sample stage will be isolated with ceramic washers and the linear feedthrough will be isolated with a ceramic sleeve. The plate will be isolated to allow the acceleration voltages up to 10 kV.

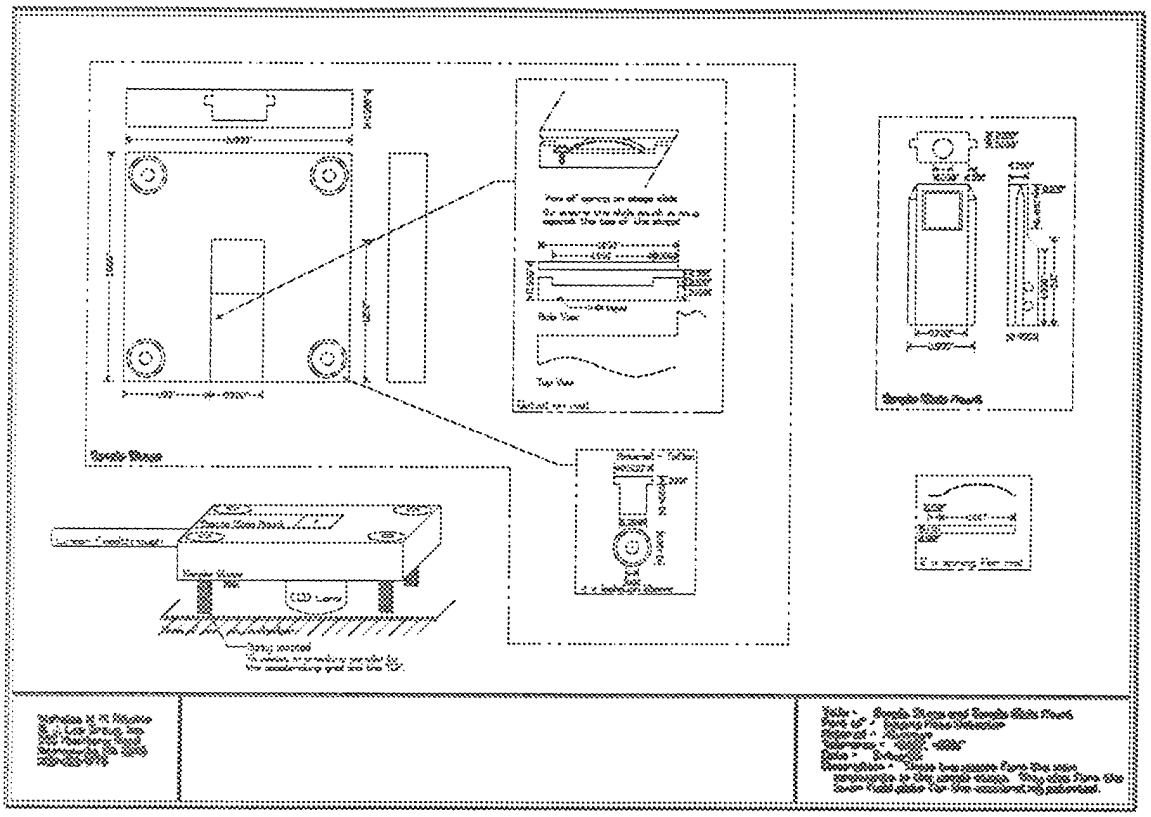

Figure F.1 - Sample stage

Feature 3 is implemented by mounting the sample slide in an indentation which aligns the top surface of the sample with the top of the stage and by making the surface of the stage flat across a 3" square area.

Feature 4. is to be implemented in the future by routing liquid nitrogen through the base portion of the sample mount. This will not be implemented until Phase III.

The Fission Fragment Source Configuration

The choice of fission fragment source and source location effects many different aspects of the instrument performance and safety. The most critical of the performance issues is the imaging time. The less time the instrument requires to expose an image, the greater the utility of the instrument.

A useful relationship to keep in mind while considering the source is the relationship between source activity, source-to-sample distance and desorption events on a 1 mm^2 sample.

> A 1 mm^2 sample will be struck ~9 times/second with fragments from a 1 μCi source located at 1". As the distance from the source to the sample increases, the desorption rate decreases as the square of the distance. A 100 × 100 matrix would require ~19 minutes to expose to an average of 1 desorption per pixel.

Of course, due to the random nature of the desorption process the distribution of desorption events will not be uniform pixel-to-pixel. When a better exposure is required the exposure time can be increased. In this instrument, we envision the image will develop in real-time on the computer monitor and the operator can decide when the exposure is sufficiently good.

To optimize performance, we want a source with the following characteristics:

(1) High activity to reduce image exposure times

(2) Located close to the sample to reduce image exposure times

(3) Sufficiently thin to permit fission fragments to escape from both sides with negligible energy loss

However, to keep the instrument safe we would like to keep source activity to a minimum. While sources are readily available with activities up to 50 μCi we would like to design our instrument around a 10 μCi source. In keeping with the goal of using off-the-shelf parts whenever possible, we have designed our instrument around the 10 μCi fission fragments source available from Isotopes Product Laboratories.

Clearly, the optimal location for the fission fragment (^{252}Cf) source is close to the sample. The design we are proposing has the source within 1" of the sample. This makes the region between the source and the sample very tight. Figure F.2 shows a scaled drawing of the source-sample region in the telescoping instrument. One scintillator, a front surface mirror to assist in imaging the scintillator, and the acceleration plate/grid are located between the source and sample.

Start Detector

To permit precise measurements of the time-of-flight of desorbed ions, a high resolution start signal is required. As is common practice in PDMS, we intend to use a microchannel plate to time the recoil fission fragment.

This assembly is located on the opposite side of the source from the sample. It consists of a thin metal conversion foil to convert the fission fragment into a pulse of approximately 80 electrons and a microchannel plate (MCP). The MCP we have chosen is a Galileo model TOF-250. This MCP impedance is matched to a 50 Ω signal output to optimize the timing characteristics. Figure F.3 is a scaled drawing showing the location of the start detector with respect to sample and source.

Acceleration Plate

The acceleration plate is located between the lower scintillator and the sample. The acceleration plate is a 3" × 3" plate with a 4 mm hole through the center for the flight tube leading to the time-of-flight. The acceleration plate is flat and aligned exactly parallel to the sample plate forming a parallel plate capacitor. Off to the side of the flight tube and next to the lower scintillator is an additional hole through which the fission fragments pass. The two holes in the base of the acceleration plate disrupt the electric field line and would cause the ions to deviate from the correct trajectory up the time-of-flight tube. To correct this, the base of the acceleration plate around the holes is covered with a 90% transmission nickel mesh.

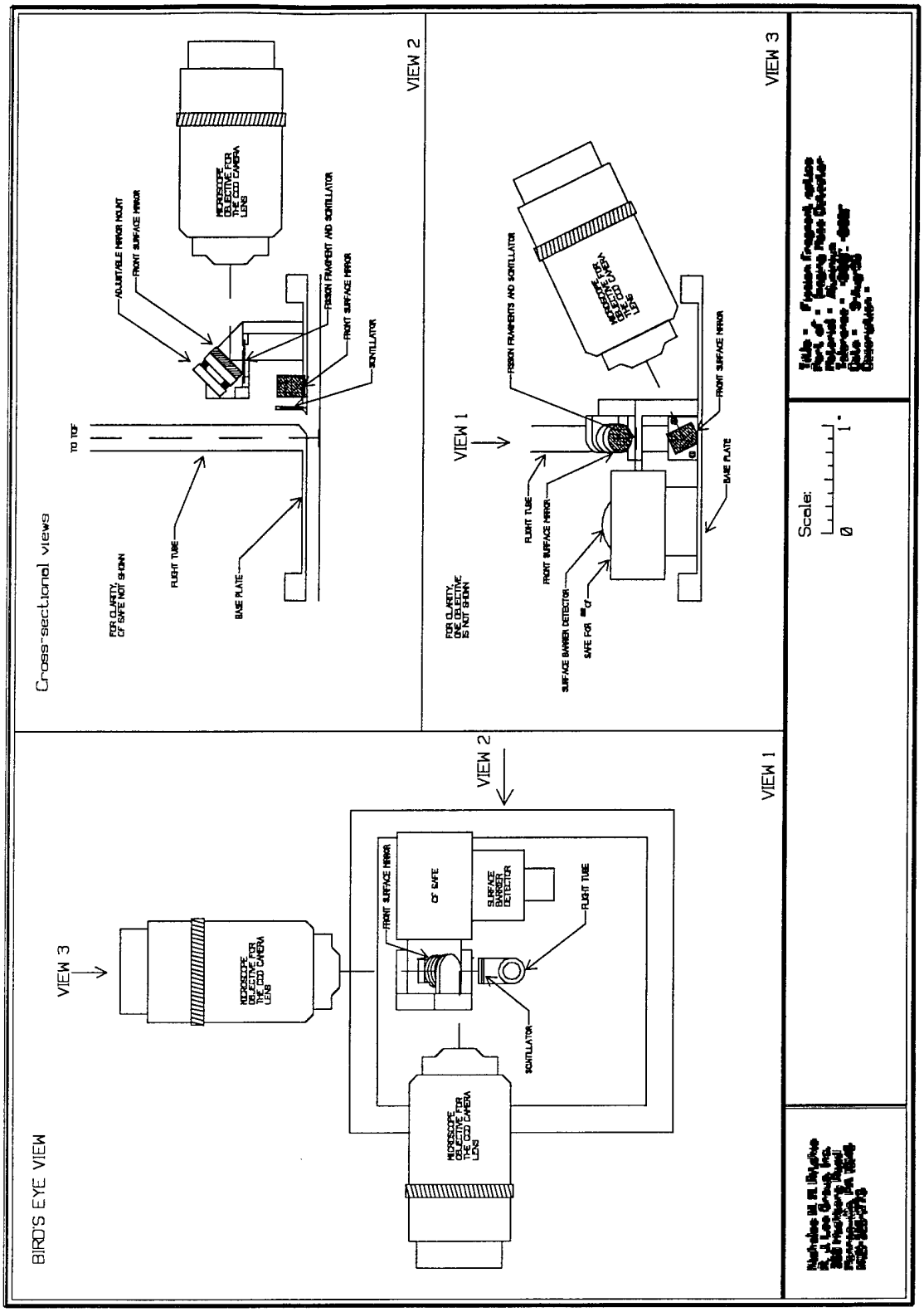

Figure F.2 - Source, sample, telescope region

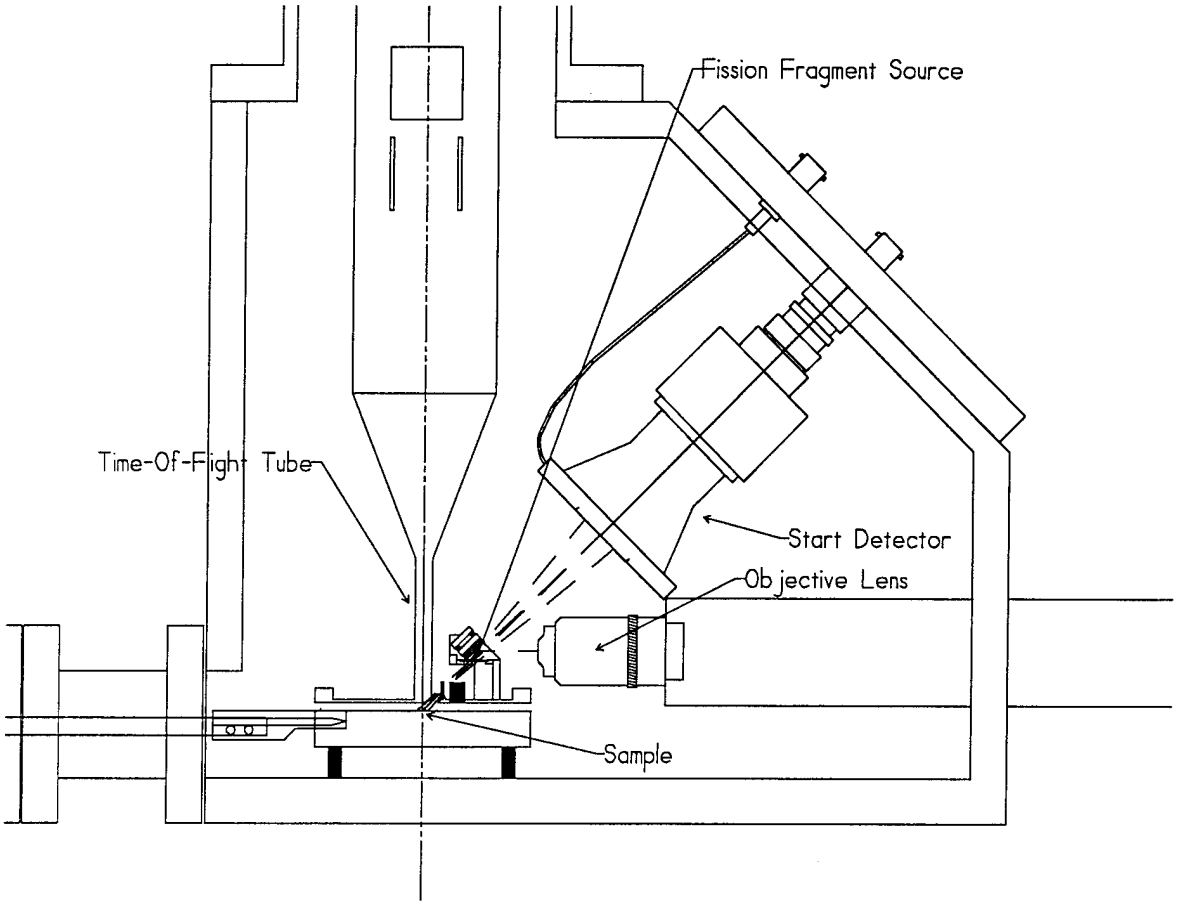

Figure F.3 - Source, sample, start detector

Appendix G - Evaluation of Position Sensitive Detectors

A number of PSD technologies have been developed commercially to meet the needs of the experimental particle and nuclear physics communities[12]. Some of these technologies are based on semiconductor devices, others on gas ionization and others on scintillators. We have investigated the available technologies to determine which (if any) might be applicable to our instrument. We would much rather purchase a proven off-the-shelf item than develop our own detector. Of these technologies, the semiconductor and scintillator devices offer the most promise.

Silicon-Based

A number of distinct silicon-based technologies are available including the silicon microstrip detector and the silicon drift chamber. The most promising of these is the silicon microstrip detector[13]. The silicon microstrip detector consists of an ~300 μm thick block of n-type doped silicon. On one side of the block strips of a p-type doping material is implanted into the silicon block. These strips are typically 10 μm wide and spaced by 25 μm center-to-center and form a diode junction. On top of each diode junctions a conducting read-out strips are etched . The other side of the silicon block is coated with conducting material and the detector is biased. A charged particle passing through a silicon microstrip detector forms electron-hole pairs in the doped silicon. The bias field attracts the electrons towards the readout strips. The electrons are read out by measuring the current on each conducting strip.

The silicon microstrip detector played a major role in the recent discovery of the top quark. Resolutions of 10 μm are easily achieved and recently, using sophisticated charge division techniques resolutions of 1 μm have been demonstrated.[14]. The limitations of microstrip detectors include the complexity of the readout electronics, the fragility and thickness. Each readout strip on a microchannel plate requires its own amplifier for the most accurate positioning. When the strips are spaced at 20 μm this requires 50 charge sensitive amplifiers per mm per dimension. This can be prohibitively complex and expensive. The microchannel plate is also susceptible to damage from the fission fragments. Most damaging to the utility of the microstrip detector is the detectors thickness which is typically 300 μm. For a minimum ionizing particle such as found in an accelerator experiment 300 μm is not thick. However, since fission fragments interact so strongly 300 μm is at least an order-of-magnitude too thick to permit the passage of fission fragments.

In a silicon drift chamber[15], much like in a microstrip detector, the passage of a charged particle causes electron-hole pairs to form in the doped-silicon body. In a silicon drift chamber,

---

12 L. Struder, L. Nucl. Inst. & Meth. in Phys. Res. **A283**, .3 (1989) p.387-98

C. F. G. Delaney, E. C. Finch Radiation Detectors, (Clarendon Press, Oxford 1992)

13 A. M. Litke and A. S. Schwartz, Scientific American, **227**, 5 (1995) p. 77

14 J. Straver, O. Toker, P. Weilhammer, C. Colledani, W. Dulinski, R. Turchetta, L. Bosisio, Nucl. Instr. & Meth. in Phys. Res. **A348** Iss: 2-3 (1994) p. 485-90

15 G. Hall, Nucl. Inst. & Meth. in Phys. Res. **A273**, 2-3 (1988) p.559-64

however, the position of the charged particle is deduced from the time it takes electrons to drift under the influence of an electric field to a readout strip. The electronics required for a silicon drift chamber is much simpler than for a microchannel plate. The technical literature reports resolutions of 2 μm. Drift chambers also suffer from the same fatal flaw as microstrip detectors -- they are too thick.

One alternative technology mentioned occasionally in the technical literature is the use of CCD cameras to measure charged particle trajectories. While fission fragments impacting directly on a CCD would quickly damage the CCD, a thin conversion foil which stops the fission fragment and transfers the energy into numerous less energetic electrons is a viable alternative. Without electron optics, the resolution limitation would be the CCD chip pixel spacing which is typically 10 - 15 μm.

Scintillator Based

A scintillator is a material which when struck with an energetic particle or ion gives off light. Five common classifications of scintillators are inorganic crystals, organic crystals, plastics, organic liquids, and noble gases. Of these types, organic liquids and noble gases are difficult to work with under vacuum and were eliminated from consideration for this reason. We investigated a variety of inorganic crystals, organic crystals and plastics through the literature and various bench level tests. Our goal was to identify a scintillator material which would both produce good light output from fission fragments and be capable of good spatial resolution.

Through the literature we identified a variety of potential scintillator materials [see references at end of this appendix]-- ZnS(Ag), Bicron BC-400, Bicron BC-404 and anthracene which we considered sufficiently promising to warrant bench-level tests. ZnS(Ag) is a white opaque inorganic crystal. ZnS(Ag) is readily available in a powder with typical grain size of less than 10 μm. Bicron BC-400 and Bicron BC-404 are commercially available plastic scintillators. They have properties very similar to Pilot-B and NC-104 both of which are often mentioned in the literature. Anthracene is an organic crystal.

Most of the technical literature on scintillators discusses the interaction of various scintillator materials with x-rays, γ-rays or β-particles. Very few articles discuss α–particles and even fewer discuss fission fragments. In general, however, it can be said that most scintillators will give off significantly less light for a heavy ion than a β-particle of the same energy. The reason for this is simply because the heavier ions deposit too much energy in too small a volume saturating the scintillator output. The additional energy is carried off as thermal energy.

Ultimately our study of the literature left us with some unanswered questions about the light output of various scintillators and the imaging resolution we could hope to achieve. To fill in these gaps, we developed a series of experiments, which are detailed in later appendices.

Appendix J discusses techniques we used to construct or mount the various types of scintillators.

Intensified CCD Cameras

The scintillator is not inherently a position sensitive detector. It must be read out by some type of imaging detector. Various options are available the most promising of which are derived from the CCD camera. A good standard CCD camera is capable of imaging in light levels down to 0.1 lux. Add an image intensifier to a CCD camera and the CCD camera is capable of imaging in light levels of 10^{-6} lux. The additional sensitivity of an intensified CCD camera is necessary to image single scintillations.

An image intensified CCD (ICCD) camera is mot much different from a high quality CCD camera with an image intensifier front end. An image intensifiers is like a position sensitive photomultiplier tube (PMT). Similar to a PMT, an image intensifier has a photocathode which is sensitive to light. When a single photon strikes the photocathode, it will knock off a single photoelectron with probability equal to the *quantum efficiency*. The quantum efficiency varies with the frequency of the incident light and the material and construction of the photocathode. An electric potential between the photocathode and an electron multiplier accelerates the electron towards the electron multiplier. In an image intensifier, the electron multiplier is a microchannel plate (MCP). A MCP consists of a highly resistive material with hundreds of thousands of ~10 μm of through channels. An electric field is applied between the faces of the MCP. When an electron strikes the MCP, the electron on average liberates $n >> 1$ electrons from the surface. These electrons are accelerated through a channel in the MCP towards the other face. Most of the electrons will strike a side of the channel and liberate additional electrons. Like a PMT, the single incident photo-electron cascades into hundreds of thousands of accelerated electrons. The actual number of electrons in a cascade pulse is a function of the voltage applied across the faces of the MCP. Higher voltages lead to higher charge gain. The cascade electrons strike a phosphor located close to the output plane of the MCP. The resulting light flash on the phosphor is imaged with a CCD camera.

The CCD camera is coupled to the phosphor either with lens or with fiber optics. Lens systems project images of the phosphor onto the camera but are less efficient than fiber optics and tend to produce a camera with less sensitivity. Fiber optically coupled cameras use a bundle of fiber optics which is optically coupled to the intensifier and the CCD camera to transfer light from the phosphor to the CCD chip. The fiber optics may be tapered between the intensifier and the camera to allow a smaller CCD chip to be used with a larger MCP. MCP's typically come in either 18 mm, 25 mm or 40 mm diameters.

Image intensifier technology is further divided into Gen. I, Gen. II or Gen. III to describe the generation of the technology. Gen. III is the most sophisticated and is the current state of the art. Gen. III uses a GaAs MCP and has smaller channel size and thus higher resolution that either Gen. II or Gen. I. Gen. I is not based on the MCP and few cameras are available with Gen. I. These devices should be avoided. Gen. II is a compromise. A good Gen. II can almost perform as well as a Gen. III.

Generation	Material	Resolution (line pairs/mm)
Gen. II		32
Gen. III	40	

Table G.1 - Image Intensifier Technologies

Many different types of photocathode materials are available, each suited better to a specific wavelength region. Most photocathodes are better in the red region of the visible spectrum and ZnS(Ag) scintillates around 450 nm and plastic scintillators scintillate around 400 nm -- in the blue. However, photocathodes are available which operate with reasonable efficiency at these wavelengths. Lumogen enhanced photocathode are capable at wavelengths in the near-UV (290 nm).

MCP's are available directly from Galileo and image intensifiers are available from Phillips, RCA, Hamamatsu, Loral-Fairchild and other companies. Neither of these products are ready to be used off-the-shelf. Rather than reinvent the wheel it is better to purchase an off-the-shelf CCD camera. These are available from Philips, Xybion, Stanford Photonics, Princeton Instruments, and Loral-Fairchild. Typically, they cost between $10,000 and $25,000 depending upon the sophistication of the camera.

A CCD camera can control its exposure time by controlling how long the capacitors at each pixel sum the incoming signal. On a standard CCD camera, it will typically offer electronic shutters of either 1/2000 or 1/60 of a second. Intensified CCD cameras, by taking advantage of the nano-second rise times of MCP's, are capable of much more precise gating. By pulsing the applied bias voltage on the MCP, it is possible to essentially turn the CCD camera on/off in time scales as short as 5 ns. This feature is critical for imaging events of short duration in an intense background light level.

The less expensive ICCD cameras use the standard RS-170 composite video output standard. This standard implements *fields* consisting of either the odd or even CCD chip scan lines. Each field is scanned out in 1/60 of a second. Two fields consisting of odd and even scan lines are scanned out each 1/30 of a second to form a *frame.*

Because the image is divided into two frames which do not actually image the same time

Photocathode Material	Luminous Sensitivity (at 450 nm)
Gen. II (Red)	38 mA/W
Gen. II (UV)	42 mA/W
Gen. III	~0
Gen. III (Blue)	50 mA/W
Gen. III (NIR)	~0

Table G.2 - Summarizes the luminous sensitivity of various common intensifier photocathode materials

period, we can not use a RS-180 standard camera. It is possible to miss events in one field that occur while the other field is imaging. Higher end cameras are capable of reading out a full frame at one time.

While we can not predict when a fission event will occur, we know immediately after such an event has taken place. The ICCD camera in this instrument should have an option to integrate until an event occurs and read out the frame immediately after.

An alternative to intensified CCD cameras for low intensity imaging are low noise, slow scan cooled CCD cameras such as manufactured and sold by Princeton Instruments. These cameras cool the CCD chip to below 0° C and use ultra-low noise slow scan read-out electronics. These cameras are available in formats of up to 2024 x 2024 but serve a different purpose than ICCD cameras. They are useful for events of long duration which can be integrated to decrease noise levels. Scintillation events do not fall into this category and these cameras are not really very useful for us.

References

C. B. Franklyn, "Fission fragment response characteristics of thin film plastic scintillators", Nucl. Instr. & Meth. in Phys. Res. B35, no.3-4 p.315-18

I. Kanno, Y. Nakagome, "Response characteristics of thin film detectors to fission fragments", Nucl. Instr. & Meth. in Phys. Res. A251, no.1 p.108-14

C. Manduchi, M. T. Russo-Manduchi, G. F. Segato, "Response of ulta-thin scintillator foils to fission fragments", Nucl. Instr. & Meth. in Phys. Res. A243, (1986) no.2-3 p.453-8

B. K. Batra, A. C. Shotter, "Passage of fission fragments through thin film plastic scintillators", Nucl. Instr. & Meth. in Phys. Res. B233, (1984) no.1 p.14-19

N. N. Ajitanand, "A semi-empirical expression for specific luminescence in plastic scintillators", Nucl. Instr. & Meth. vol.143, (1977) no.2 p.345-7

B. K. Batra, A. C. Shotter, "Response of thin film plastic scintillator to fission fragments", Nucl. Instr. & Meth. vol.124, (1975) no.1 p.101-6

G. Lanzano, et al. "Heavy ions detections by using BaF/sub 2/ crystals coupled to thin plastic scintillator", Nucl. Instr. & Meth. in Phys. Res. vol.A323, (1992) no.3 p.694-6

P. D. Goldstone, R. E. Malmin, F. Hopkins, P. Paul, "Development of thin-film plastic scintillator detectors for use in in-beam fission studies", Nucl. Inst. and Meth. vol.121, (1974) no.2 p.353-8

L. Muga, A. Clem, G. Griffith, H. S. Plendl, R. Eaker, R. Holub, "Luminescence response of thin plastic scintillator detectors to fission fragments from proton-induced fission of ^{232}Th, ^{235}U, and ^{238}U", Nucl. Instr. & Meth. vol.119, (1974) no.2 p.255-60

P. D. Goldstone, R. E. Malmin, F. Hopkins, P. Paul, "Development of thin-film plastic scintillator detectors for use in in-beam fission studies", Nucl. Instr. & Meth. vol.121, (1974) no.2 p.353-8

W. J. McDonald, A. I. Kilvington, C. J. Batty, J. L. Weil, "Identification of fission activity using thin-film detectors", Nucl. Instr. & Meth. vol.115, (1974) no.1 p.185-8

M. L. Muga, D. J. Burnsed, W. E. Steeger, H. E. Taylor, "A new time-of-flight particle detector", Nucl. Instr. & Meth. vol.83, (1970) no.1 p.135-8

Appendix H - Impulse Detectors

We also made some preliminary but unsuccessful tests of a novel position sensitive detector proposed by Dr. William Ulbricht. The impulse PSD (IPSD) is a novel position sensitive detector which proposes to use the compression wave impulse from the impact of an energetic fission fragment to locate the impact location in two-dimensions.

The detector we envision would consist of a thin (~1 μm) membrane through which the energetic fission fragment pass. As the fragment traverses the membrane it instantaneously heats the localized region around the impact location. We believe that this heating process would cause the material to expand and the expansion would lead to a compression wave radiating out from the impact location. Three or more impulse detectors located around the edge of the membrane would record the arrival time of the compression wave. The impact location can be deduced from differences in the arrival time.

The idea is particularly appealing due to its simplicity. While simple in principle, implementing it may be more difficult. We made some initial attempts to implement an IPSD using ceramic piezoelectric detectors. The detector we built used a 1" square aluminum membrane with 4 piezo-electric transducers located on each of the four edges of the foil. The foil was stretched tight with four springs mounted in a square frame. The response of a piezo crystal to an impulse is a current pulse which we preamplified with a Dawn Electronics Model DN-620 charge sensitive preamplifier and amplified with a series of National Instruments 9618 op-amps. The system was mounted in a simple vacuum system and was tested with α-particles.

With this system we were unable to identify any impulses which we could unambiguously attribute to the α-particles. The most significant limitation was the sensitivity of the instrument to room vibrations. Despite our modest attempts to isolate the system from the room vibrations, we were unable to achieve the ultimate level of sensitivity determined by the piezo-electric crystals and the electronics. The vacuum system did help to eliminate any microphone-like pickup from the air however we were unable to isolate the detector from the vibrations which coupled in through the floor.

While our initial attempts to implement an IPSD did not succeed we believe that this technology still holds promise. The main problems with the system we developed were

(1) The system was too sensitive to vibrations

(2) The system may have been insufficiently sensitive to impulses.

Each of these problems can be addressed. In fact, much of the technology necessary is standard to the atomic force microscopy (AFM) community. AFM's must be carefully vibration isolated from the environment. This is often achieved by hanging the system from multiple springs and rubber cords. Careful attention is paid to identifying and eliminating any resonant frequencies. Similarly, the sensitivity of the system can be increased using an optical interferometric system for measuring motion of the membrane surface. The outline for such a system is shown in Figure H.1. In this system, the motion of the mirror mounted on the membrane is measured using a fiber optic Mach-Zender interferometer. Potentially an interferometer such as this is capable of

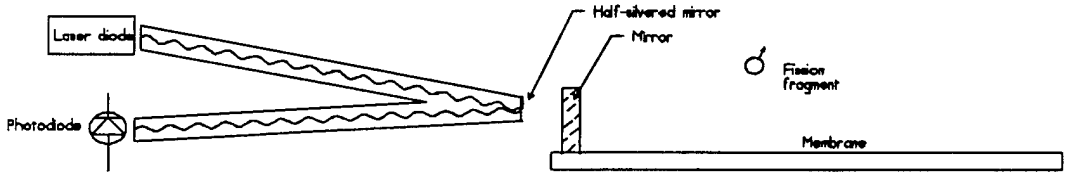

Figure H.1 - An interferometric impulse detector for the impulse position sensitive detector

measuring motions as small as a couple nano-meters. A similar configuration has proven very successful in microphones in regions of high electrical noise.

We are optimistic about an IPSD based on a Mach-Zender interfermometer and we intend to test such a system in the future.

Appendix I - Imaging methodologies

While the components of the telescopic imaging system have been discussed elsewhere, the overall implementation of the imaging system and how it will be integrated with the time-of-flight spectrometer has yet to be discussed. This appendix covers these issues.

Figure I.1 shows a simple schematic diagram of a scintillator, camera and associated image acquisition electronics. To optimize the instrument speed, we would like to have one and only one fission fragment event per frame of video data. Since the fission events occur randomly, it is hard to know when a fission event has occurred. To ensure we get one and only one fission event per frame, we need some type of trigger to indicate when a fission event has occurred. The video output from the CCD camera is not a good choice. The entire frame must be read out to determine whether one event has occurred and there is no way to ensure that only one event will have occurred. If two events have occurred the data must be discarded since there is no way to tell which fragment caused which desorption.

Optimally, what we would like is some kind of trigger that will measure the light output from the scintillator and whenever a bright flash, due to a fission event occurs, the trigger would start the CCD camera video readout. One could imagine using a photomultiplier tube (PMT) to provide the trigger. The output of the PMT would be monitored and whenever a sufficiently bright pulse occurs, the ICCD camera would read out a frame. Due to the tight spatial constraints near the scintillator it is hard to get a PMT sufficiently close and it may not be necessary.

The image intensifier stage of the ICCD camera is already very similar to a PMT. Both amplify weak light signals with a photocathode and a high-voltage electron multiplier. Image intensifiers are not typically designed to be used like a PMT. Electrons from the electron

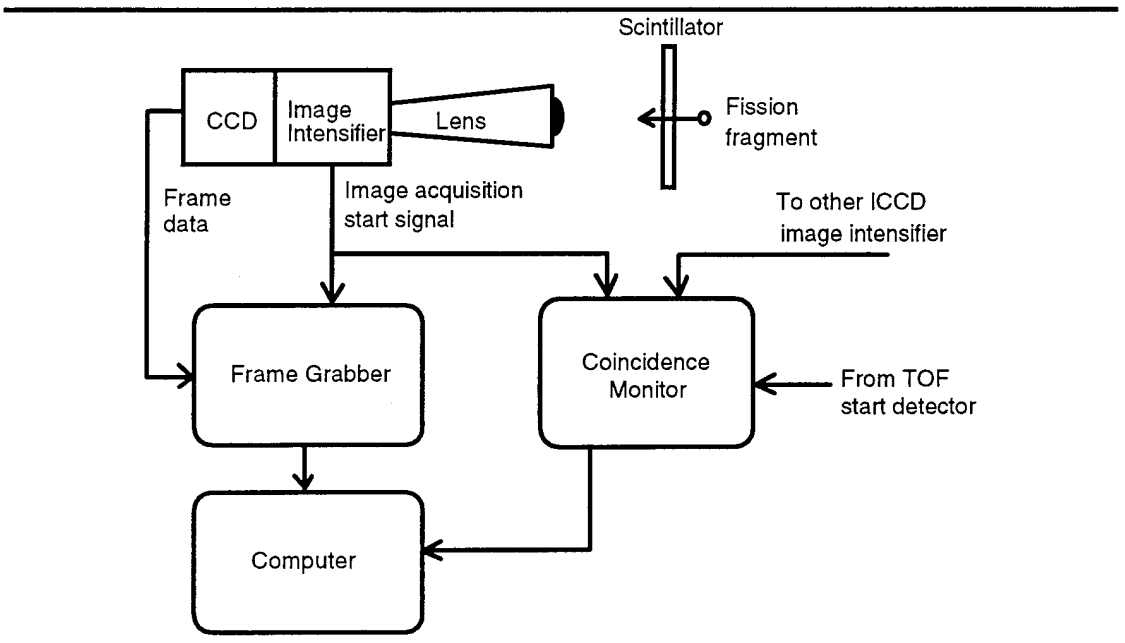

Figure I.1 - Overview of the image acquisition and event determination system

multiplier in an image intensifier are not collected on an anode as is the output signal from the PMT dynode chain. The electrons in an image intensifier strike a phosphor plate which is imaged with the CCD camera. There is an alternative way to use an image intensifier as a light sensitive detector. Whenever a bright flash occurs on the image intensifier, the current draw on the high voltage power supply will increase to replace the depleted charge on the microchannel plate. By monitoring the high voltage power supply for increased current demand, it is possible to determine when a bright flash has occurred on the sample.

Figure J.1 shows how we implement a system around this signal. The frame grabber receives two signals from the image intensifier on the CCD camera -- the video signal and the current signal. Whenever the current signal from the image intensifier exceeds a discriminator level, a logic level pulse triggers the frame grabber to acquire a video frame.

The trigger from the image intensifier also goes to a coincidence monitor. The coincidence monitor assures that all the necessary events for a good measurement occur simultaneously. To acquire a single imaged time-of-flight spectrum, the following three events must occur.

(1) a fission fragment must be imaged simultaneously on both scintillators

(2) a simultaneous start signal must occur on the TOF start detector

The purpose of the coincidence monitors is to ensure these events occur simultaneously and to discard events which do not match these criteria. The coincidence monitor receives triggers from both ICCD cameras and the TOF start detector and outputs a signal back to the computer to indicate when a good event occurs. The computer is responsible for collecting the data for good events including grabbing images of both scintillators, analyzing these images to extract two positions: extrapolating to the impact location and recording a time-of-flight spectrum. The data for each event will comprise of an (X,Y) pair with the impact location and list of the masses

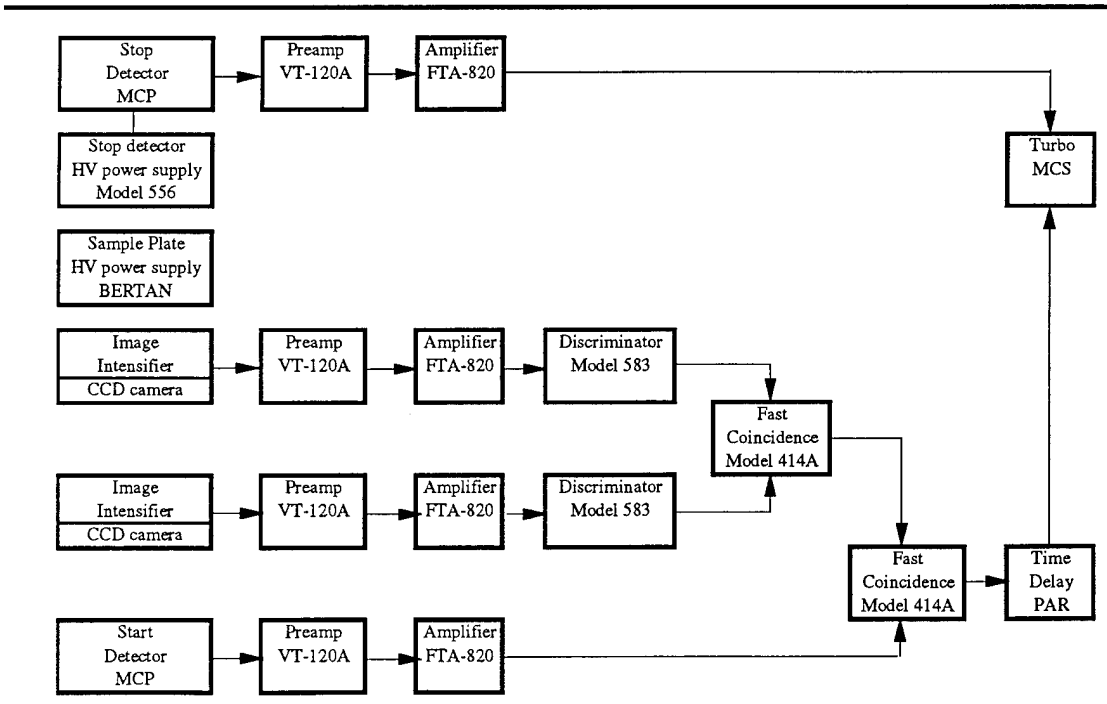

Figure I.2 - Overview of timing/coincidence electronics

Supplier	Item	Model	Qty	Cost (each)	Line
EG&G Ortec	NIM Bin + Power supply	4001C/D	1	$2,260	$2,260
EG&G Ortec	Preamplifer	VT-120A	4	$350	$1,400
EG&G Ortec	Fast timing amplifier	RTA-820	4	$1,165	$4,660
EG&G Ortec	Constant fraction discriminator	583	2	$2,100	$4,200
EG&G Ortec	Fast conincidence	414A	2	$995	$1,990
EG&G Ortec	Turbo MCS - multichannel scaler	T914	1	$7,425	$7,425
EG&G Ortec	Stop detector HV power supply	556	1	$1,370	$1,370
Bertan	High voltage power supply		1	$2,000	$2,000
Princeton Applied Research	Time delay		1	$2,000	$2,000
				Total	**$27,305**

Table I.1 - Timing electronics

measured by the time-of-flight. The data for a mass image will comprise of a list of many event data points.

Appendix J - Scintillators and Scintillator Preparation

Five common scintillator classifications are inorganic and organic crystals, plastics, organic liquids and noble gases. Of these types, organic liquids and noble gases are difficult to work with under vacuum and will not be considered.

Tables J.1, J.2 and J.3 summarize the properties of some common inorganic, organic and plastic scintillators. The information in these tables were collected from the following sources[16]. Most often the efficiency quoted refers to the efficiency for β-particles. However, in a couple of cases, particularly those scintillators which are particularly good for heavier ions, the α–particle efficiency is quoted.

Both organic and inorganic scintillators have been used for the detection of fission fragments but neither is particularly well suited[17]. The pulse height from fission fragments on CsI(Tl) is only a factor of two greater than from Po^{210} alphas[18].

The single most efficient scintillator for α–particles and fission fragments listed in these tables is ZnS(Ag). ZnS(Ag) is available as polycrystalline powder with grain sizes of < 10 μm (from Osram-Sylvania among others.) Unlike certain other inorganic crystal scintillators, macroscopic crystals are not available. ZnS(Ag) is opaque to it's own scintillation light.

The plastic scintillators such as Bicron BC-400 and BC-404 are also promising materials. These are similar to the often mentioned NE-102 and Pilot-B. Plastic scintillators tend have fast decay times but less light output than inorganic scintillators. Plastic scintillators can be molded or machined into a wide variety of shapes.

The Scintillation Process in an Inorganic Crystal

The scintillation process in an inorganic crystal is a solid state process involving the band structure of the crystal. The incident particle is slowed by the crystal electrons resulting in ionization and excitation of the crystal lattice. The energy deposited in the crystal migrates to an activation center and is stored. The energy may be stored in an activation center for time periods extending from nanoseconds to many minutes depending upon the scintillator properties. Eventually, the energy is emitted as a photon or as thermal excitation of the lattice.

---

16 Bicron Product Literature, Bicron Inc. Newbury, OH (216)-564-2251

G. Knoll, Radiation Detection and Measurement, (J. Wiley, New York, 1979)

Hamamatsu Product Literature, Hamamatsu, Bridgewater, NJ (908)-231-0960

Scintillation Counters

Bridgman-Stockbarger, Rev. Sci. Inst. **7**,133 (1936)

Buck & Swank, Nucleonics **11**, #11, 48 (1953)

17 Meyer and Murray, IRE Trans. Nuclear Sci, **NS-7**, 22 (1960)

18 C. B. Fulmer, Phys. Rev. **108**, 1113 (1957)

J. S. Fraser and J. C. D. Milton, Nuclear Instruments **3**, 275 (1958)

Material		Time (s)	Centered (nm)	(g/cc)	Efficiency	
NaI(Tl)		0.3 us	4.20E+02	3.67	0.13	Gamma ray & charged particle spectroscopy
NaI	at -188 C	0.06 us	300	3.67	0.25	low-E gamma and charged particle spectroscopy
CsI(Tl)		0.43 us for alphas	max. in red	4.51	less than NaI	Gamma ray & charged particle spectroscopy
CsI	at -188 C	0.6 us	400	4.51	0.35 for alphas	
LiI(Eu)		1.1 us	470	4.06	1/3 of NaI(Tl)	high efficiency for slow neutrons
KI(Tl)		> 1 us	410	3.13	1/4 of NaI(Tl)	charged particle detection
CsF	unactivated	0.2 us for alphas	425	3.59	v. weak for alphas	fast detector for g
ZnS(Ag)		< 1 us	450	4.1	0.28 for alphas	detection of alphas and fission fragments
$CdWO_4$		0.5 us	530	7.9	less than NaI(Tl)	possible gamma detector

Table J.1. - Summary of inorganic crystal scintillator properties

Preparation of ZnS(Ag) Screens

While the conversion efficiency of ZnS(Ag) for heavier ions is clear, the preparation of the scintillator screen is also critical. Formulating ZnS(Ag) screens comes with its own unique challenges. In particular, ZnS(Ag) is opaque to its own radiation and thus the screen must be sufficiently thin so that a reasonable fraction of the resulting light can escape. However, the screen can not be too thin or else the ZnS(Ag) will not cover 100% of the surface. Regions will exist which when struck will not produce light.

We tried numerous different techniques for developing our own ZnS(Ag) screens and found a number of commercial ZnS(Ag) screens. The paragraphs below discuss the commercial screens and the best of the screens we developed.

Commercial ZnS(Ag) Screens

Tuff-Tector - the Tuff-Tector is ZnS(Ag) embedded in epoxy. The sample of the Tuff-Tector material we tested was provided by Dr. Stepanie McElhaney of RIS Corp[19]. We do not know the exact composition.

ZnS(Ag) embedded in mylar - this sample was provided by Dick Landfried of W. B. Johnson and Associates[20].

---

19 RIS Corp. Oak Ridge, Tennesse (615)-927-6708

Scintillator	Decay time (s)	Emission Centered (nm)	Density (g/cc)	Conversion efficiency
Anthracene	30 ns	440		0.05
Trans-stilbene	4-8 ns	410		1/2 of anthracene
Quaterhenyl	4 ns	440		0.9 of anthracene

Table J.2 - Properties of various organic scintillators

ZnS(Ag) embedded in mylar - this sample was provided by Dick Landfried of W. B. Johnson and Associates[20].

Proprietary ZnS(Ag) Screens

ZnS(Ag) in epoxy on a glass microscope slide

(1) The ZnS(Ag) is prepared by grinding in a ball mill to reduce the grain size from 10 μm (max.) to 1 μm (max.). The smaller grain size allows for thinner more consistent layers of epoxy and will probably allow for better resolution. The smaller grain size might decrease light output.

(2) The ZnS(Ag) is mixed with Epo-Tech 301-2 epoxy to form a thin paste. The paste should contain sufficient epoxy to ensure the paste spreads easily and the ZnS(Ag) bonds well to the glass surface. However, the paste must not contain too much epoxy or the majority of the fragment energy will get deposited in the epoxy rather than the scintillator

(3) The paste is spread evenly on a glass microscope slide using a razor blade. The resulting layer should be just barely thick enough to be opaque. If the layer is too thin, the coverage of ZnS(Ag) is not complete. If the layer is too thick, the screen is not transparent to its own radiation.

Preparation of Plastic Scintillator Screens

While plastic scintillators are available in many different shapes and sizes including custom shapes, the only way to get ultra-thin plastic films is to make them yourself. Fortunately, NE-102 and Pilot-B plastic scintillators can be readily formed into ultra-thin layers using the following technique[21]. BC-400 and BC-404 also work. This technique is capable of producing plastic films with stopping powers of as little as a couple hundred of $\mu g/cm^2$.

Technique for the Construction of Ultra-thin NE-102 Films

(1) Mix 6.0 g of NE-102 or Pilot-B in a solution of 50 ml of ethyl acetate plus 4.0 ml amyl acetate. In no case should the amount of amyl acetate exceed 10% of amount of ethyl acetate by vol.

---

20 W. B. Johnson and Associates, West Virginia (304)-645-6568

21 M. Muga, D. J. Burnsed, W. E. Steeger, Nucl. Instr. and Meth. **104**, (1972) 605

Scintillator	Decay time (ns)	Emission Centered (nm)	Density (g/cc)	Conversion efficiency
Polystyrene w. 16 g/l of tetraphenylbutadiene	4.6	450		0.36 of anthracene
Polyvinytolulene w. 36 g/l of p-terphenyl and 0.9 g/l of p,p'-diphenylstilbene	3	380		0.48 of anthracene
Polyvinyltoluene w. 36 g/l of p-terphenyl and 0.2 g/l of tetraphenylbutadiene	4	445		0.45 of anthracene

Table J.3 - Summary of plastic scintillator properties

(2) Allow the mix to stand for a couple hours until dissolution occurs. Transfer the supernate to a polyethylene container with a drop spout. If the film is cloudy, add amyl acetate. Too much amyl acetate makes the film "swiss-cheezy".

(3) Forming the film - Fill a 5 cm x 30 cm x 50 cm pan with 2.5-3.0 cm of distilled water at 23° C. A 10 cm x 15 cm glass plate is partially immersed at one end of the pan and inclined to an angle of 60° with respect to the surface of the water. 2 or 3 drops of the solution are squeezed out onto the center of the glass slide just above the water line. The solution will flow out over the surface until contact is made with an edge of the pan. The solvent absorbs into the water and in a couple seconds a solid film appears.

The thickness of the film may be estimated from the color of the film - from thinnest to thickest transparent, light-yellow, dull red-blue, brilliant blue, bright yellow, red, green, etc. under fluorescent light. Very thick film are transparent again.

Lift the films from the water with a 0.125" thick wire ring. (Muga used a 10 cm dia. ring.) Transfer the film to a Lucite ring (i.d. = 5.2 cm, o.d. = 6.3 cm, height = 1.0 cm) Cut away the outside portion of the film with a razor blade. The ring may be greased with optical grease to enhance the adherence of the film.

Laminates of multiple layers may be made by adding additional films to the Lucite ring. Lower the film at a slight tilt.

Aging effects may be reduced by adding additional films of VYNS or FORMVAR to each side. The films of VYNS or FORMVAR are formed in a similar manner from 4 g of VYNS or FORMVAR in 50 ml of cyclohexane.

Batra and Shotter[22] describe a variation on Muga's method for constructing NE-102 films. They use a 8 cm O-ring floated on the water to "stretch" the water surface. The uniformity of the film may be further improved by adding a second O-ring of 4.5 cm dia. when the film is nearly dry.

---

22 R. K. Batra and A. C. Shotter, Nucl. Instr. and Meth. **124**, (1975) 101-106

Appendix K - Scintillator Output Experiment

We decided to make measurements of the light output from various scintillators to better understand available scintillators. An important consideration in the choice of an optimal scintillator is the light output per incident particle, but absolute measurements of scintillator outputs are hard to find in the literature. This may be in part because it is so difficult to calibrate a detector accurately to measure light output independent of the scintillator decay time.

The experiment we developed used a photon counting photomultiplier tube and a pulse counter to measure the light output from various scintillator materials near a polonium α-particle source. A 1 cm^2 piece of each scintillator material was mounted directly on top of the α-particle source. The activity of the source was measured with a Geiger counter to be 1.17×10^3 α-particles per second over the 1 cm^2 area. The photomultiplier tube was located 3.3 cm from the scintillator and the aperture of the PMT was 6.35 mm in diameter. The geometric collection efficiency of this detector configuration was 0.92 % and the quantum efficiency of the PMT was estimated at 20%. We estimate that the measured outputs are accurate to within a factor of two. The apparatus was mounted in a black felt-lined box to exclude all room and background lights.

Results

The results are presented in Table K.1. ZnS(Ag) produced the best light output. The light output for ZnS(Cu) was hard to measure due to the large background. ZnS(Cu) tends to phosphoresce with an exponential decay time of 2-3 minutes after being exposed to room lights. We were unable to measure the fluorescence signal on top of this large background signal.. The light output from anthracene depended upon how the anthracene scintillator was prepared. A couple of materials which are not scintillators were tried to determine what the light output from these would be. They were typically at least a factor of ten less than the other scintillator materials.

Hamamatsu model 124A photomultiplier tube with HV power supply and preamp unit
Heathkit frequency counter model IM-4120
Polonium a-particle source
Techtronics 100 MHz oscilliscope
±12 V power supply

Table K.1 - Apparatus

Appendix L - Scintillator Resolution Experiments

The key to the proposed instrument is the instruments ability to spatially image scintillations due to energetic ions. To this end, we performed a number of bench-level tests to determine the feasibility of an imaging sub-system. To place some upper limits on the attainable resolution we performed a test using standard 35 mm photographic equipment to capture an image of the scintillator formed as the net result of millions of scintillations. By examining under a microscope, the photographic image sharpness of a mask imaged by the scintillator, it was possible to determine that we could expect to get resolutions of better than 30 μm with a ZnS(Ag) scintillator.

The Photographic Test

The photographic test used a standard Nikon 35 mm film camera with a lens system consisting of a 50 mm f/2.0 Nikon lens, 2 extension tubes and 4, 2, & 1 diopter close-up lenses. This combination of lenses gave a field of view of approximately 21 mm in the horizontal direction at the minimum focal distance. The scintillator was placed directly in front of the Po α–source. In air, the α–particles have a range of about 3 cm. The scintillator was placed a couple millimeters from the source. At this distance the α–particles are slightly less energetic due to collisions with the air but not by more than 10-15%. The camera was mounted in a black felt lined box to exclude light. The box was sufficiently dark to permit 24+ hour exposures without significant leakage.

We tried numerous different speeds of film in an attempt to optimize the exposure time and image resolution. It turns out that because of *reciprocity*, the tendency for activated silver salt crystals in the film to revert to their inactivated state after a period of time, the best films were in fact the slower films. ASA-3200 gains its sensitivity from the large crystal size. However, these large crystals require many photons to permanently activate. When an insufficient number strike the crystal, reciprocity causes the crystal to revert back to its inactivated state in a matter of minutes. ASA-100 has smaller crystals which require fewer photons to activate completely. Once completely activated, they do not revert back. The smaller grain size is also better for the better resolution it affords. Ultimately, we found ASA-400 to be a good compromise.

To estimate the resolution of the scintillator, we fixed grids of known spacing to the scintillator between the α-source and the scintillator material. The grid stopped the passage of α-particles. It is dark where the grid obscured the scintillator unless light is reflected off crystals in the scintillator and into the dark region. By examining the sharpness of the edges of the grid on the photographic image we could estimate the resolution of the scintillator. Light which leaks from the scintillator leaks into the region obscured by the grid and evidences itself as a less sharp gradient between dark and light.

An example photograph is shown in Figure L.1. This exposure took 24 hours. The white/light gray regions are the scintillator lit only by the light from scintillations caused by α-particles. The darker strip behind the scintillator is a metal bar located between the α-source and the scintillator. The scintillator material is a ZnS(Ag) and epoxy mix spread to form a thin (barely opaque) coat on the back of a standard light microscope slide. The size of the ZnS(Ag) crystals in this sample were <10 μm. In this figure, the circular TEM is clearly evident in black surrounded by the white of the scintillator. The TEM grid is 3 mm across. The narrowest features on the TEM grid are the cross-members. They are 90 microns wide. In the photograph, the cross-members are easily resolved. From this photograph and others, we estimated the resolution of the scintillator material at better than 30 microns. We believe this is a conservative estimate. The lack of sharpness could be due to the image being slightly out of focus.

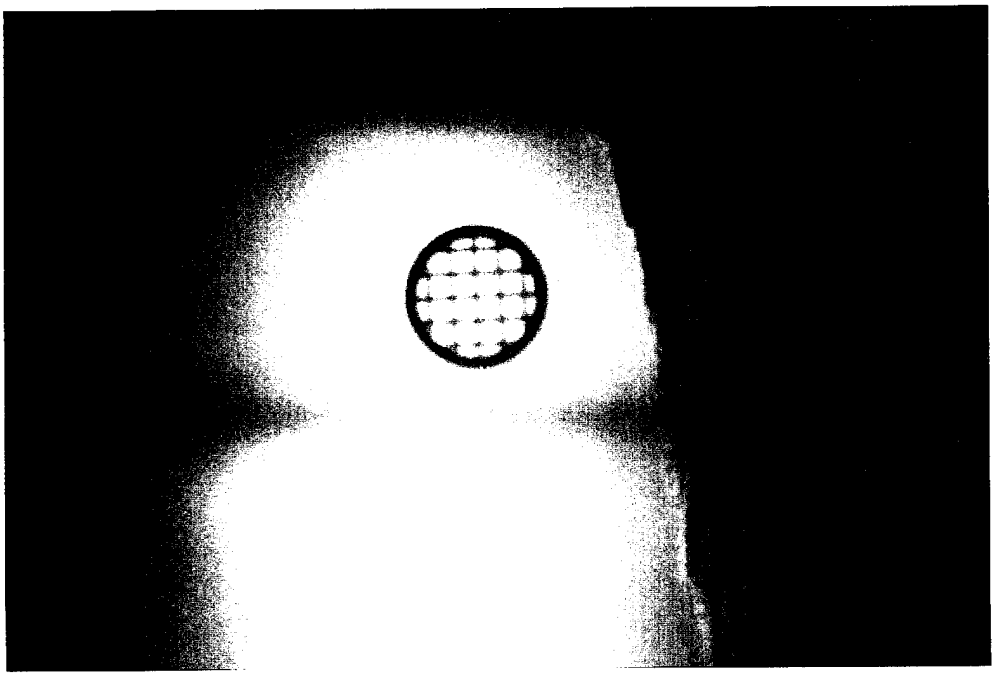

Figure L.1 - A photograph of a TEM grid on a ZnS(Ag) scintillator. The lighting for this image came entirely from scintillator light output.

Appendix M - Imaging single scintillation events

Optimistic from the results of the photographic test, we decided to acquire an intensified CCD (ICCD) camera to perform additional imaging tests. See Appendix B for details on intensified CCD camera technologies. The ICCD was an optically coupled Gen. III image intensified CCD camera -- Xybion[23] model ISS-355. The ISS-355 uses an Gen. III red photocathode and has a sensitivity of 38 mA/W at 450 nm -- the wavelength at which ZnS(Ag) fluoresces. This is quite a superlative camera. Through autogain on the intensifier and CCD camera, the camera has a dynamic range of 7 orders-of-magnitude. At the dark end of its sensitivity, the camera is specified to be sensitive to 10^{-7} lux. However the ISS-355 is not the state-of-the-art. It is an optically coupled camera and is an order-of-magnitude less sensitive than a good fiber-optically coupled camera.

The image from the ICCD is output in the standard composite video standard -- RS-170. We viewed the output on a video monitor and grabbed digital copies of the image using a SnapPlus video frame grabber. The frame grabber would convert each image into a 640 x 480 pixel image in the standard MS-Windows BMP format. Each pixel could be saved with 8-bits of gray-scale resolution where 0 is the darkest and 255 is the brightest. We wrote a C-program which is described later to analyze the BMP images.

Even with this extremely sensitive camera, the choice of high collection efficiency optics is critical. Ultimately, the important number is the collection efficiency -- the fraction of light emitted from the source which is focused and imaged by the lens system onto the intensifier image plane. To the first-order, the collection efficiency is determined by the size of the lens closest to the object. The fraction of the full 4 π stet-radians that the lens covers is approximately the collection efficiency of the lens. It is clear then that larger lenses mounted closer are likely to have better collection efficiencies than smaller lenses located further away.

We tried a number of lens systems with this camera. The first a Navitar Zoom 6000 system with a 5x Nikon microscope objective despite its excellent NA = 0.43 proved to have too poor light collection efficiency. We were not able to image single scintillations with this lens system. We attribute this to the size of the first lens, the long working distance and reflection and absorption losses in the lens system.

We also tried using an Olympus microscope with an integrated CCD camera port. This too proved unsuccessful for similar reasons as the Navitar system.

---

23 Xybion Electronic Sustems, San Diego CA (619)-566-7850

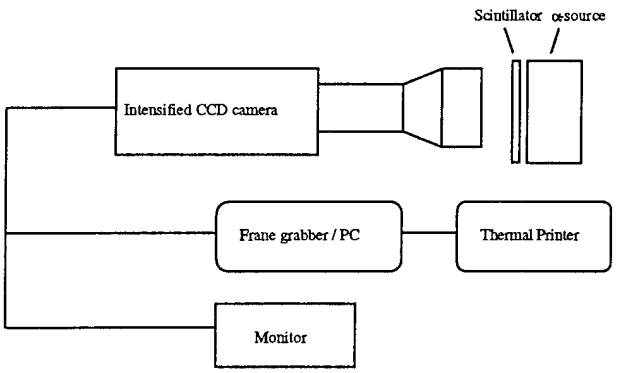

Figure M.1 - Schematic diagram of the apparatus

We were, however, successful with a system consisting of a 50 mm f/2.0 Nikon camera lens with 2 extension tubes and 4, 2, & 1 diopter close-up lenses. This system was capable of getting within 2 inches of the scintillator and yet had a very large first lens. The additional benefit of this system is the relative low cost. Since lenses like this are consumer items, they are readily available for a reasonable price. The field-of-view of this system was larger than we had aimed for -- 9 mm and this contributed to our poor resolution.

Figure M.1 shows an image acquired with this system. Each images shows one field or 1/60th of a second. The image is a negative of the screen so darker regions in the image are actually the brightest regions on the screen. The scintillator shown in these figures is the ZnS(Ag) impregnated milar film. The scintillator was located close to the α–source with a rectangular aperture between the source and the scintillator. Figure M.2 shows an image of the scintillator in room light. The four dots form the corners of the rectangular aperture. The α–source strength with the aperture in place was measured with a Geiger-Mueller counter. For this aperture, there were, on average, 240 α/s or on average 4 α per 1/60th of a second field.

Xybion ISS-355 optically couple intensified CCD camera
Commodore model 1702 composite video monitor
c-mount to Nikon photographic lens adapter
Nikon extension tubes (2)
Nikon f/2.0 50 mm photographic lens
Marumi close-up lens set (4, 2 and 1 diopter)
Snap-Plus video frame grabber
'386 Computer with Snapshot video acquisition software
Custom image analysis software
Polonium α-source

Table M.1 - Apparatus for the ICCD test

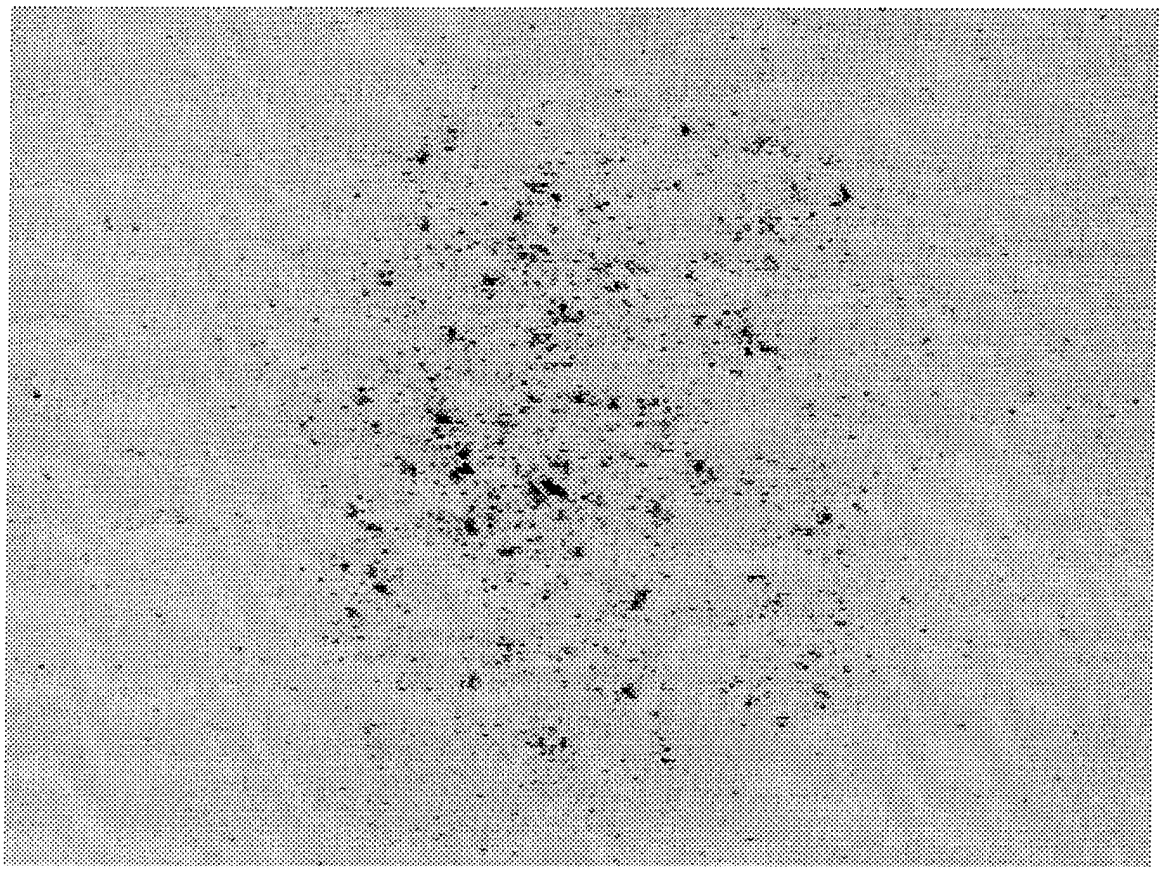

Figure M.1 - Image data from the ICCD camera. The image is a negative but otherwise unprocessed. The rectangular region visible in the center of the image is the aperture through which a-particles can strike the scintillator material.

Looking at single images, it is evident that there is significant amounts of background noise. This is to be expected. Both the intensifier and CCD gain on the ICCD camera were set at there maximum value for these images. As with a photomultiplier tube, dark noise in an image intensifier is unavoidable. At room temperature we can expect to get hundreds of thermal (**not** photo) electrons emitted from the photocathode per second. These show up as shot noise on the video screen and should on average be equally intense all over the image. The darkest spots on the Figures (the brightest on the screen) we attribute to the α–scintillations. This is because the dynamic range of the Figures is not good and it is not possible to tell which scintillations are the darkest on the Figure (brightest on the screen). Clearly, what is needed, is a program which could make full use of the 8-bit resolution of the frame grabber to differentiate between noise and scintillations. For this purpose, we wrote a simple discriminator computer program. This program reads the images and performs simple image processing.

When a histogram of the image intensity values was carefully examined it was clear that a small fraction of the pixels were significantly more bright than even the majority of the background pixels. Thus we could choose a discriminator level -- pixels with intensities above the discriminator level would be shown while pixels with intensities below this level would be set to

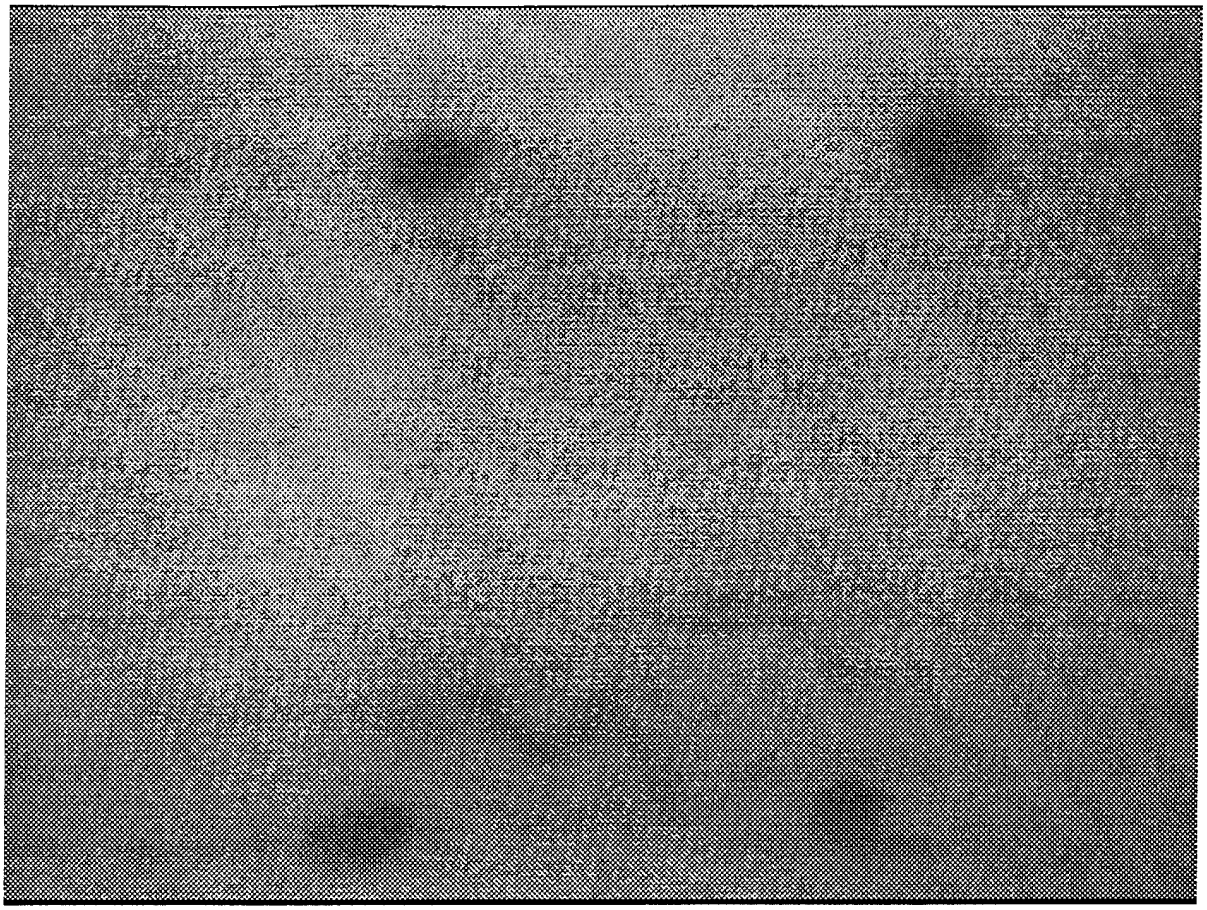

Figure M.2 - An image of the scintillator in room lights, The four dots mark the corners of a rectangular aperture in the α-particle source below the sheet of ZnS(Ag) impregnated mylar.

zero. This proved very successful. If we made the additional requirement that of the pixel and its eight immediate neighbors at least 85% must be greater than the discriminator level for the pixel to be bright we produced images similar to the one shown in Figure M.3. These two requirements ensure that we only consider flashes which are both bright and not random isolated pixels. The condition to eliminate random isolated pixels seems important to eliminate shot noise which can be as bright, but is isolated to a single pixel.

Filtering the data in this manner, we find

(1) Flashes only occur in the region where α–particles strike the scintillator

(2) The number of scintillations we measure is consistent with the α–particle flux as measured with a Geiger-Mueller counter.

This process was repeated many times and from the results we conclude that we are able to image single scintillations due to α–particles striking a ZnS(Ag) scintillator. Since fission fragments are expected to generate brighter flashes of light than the α-particles, setting the discriminator level higher should resolve fission fragments from α-particles.

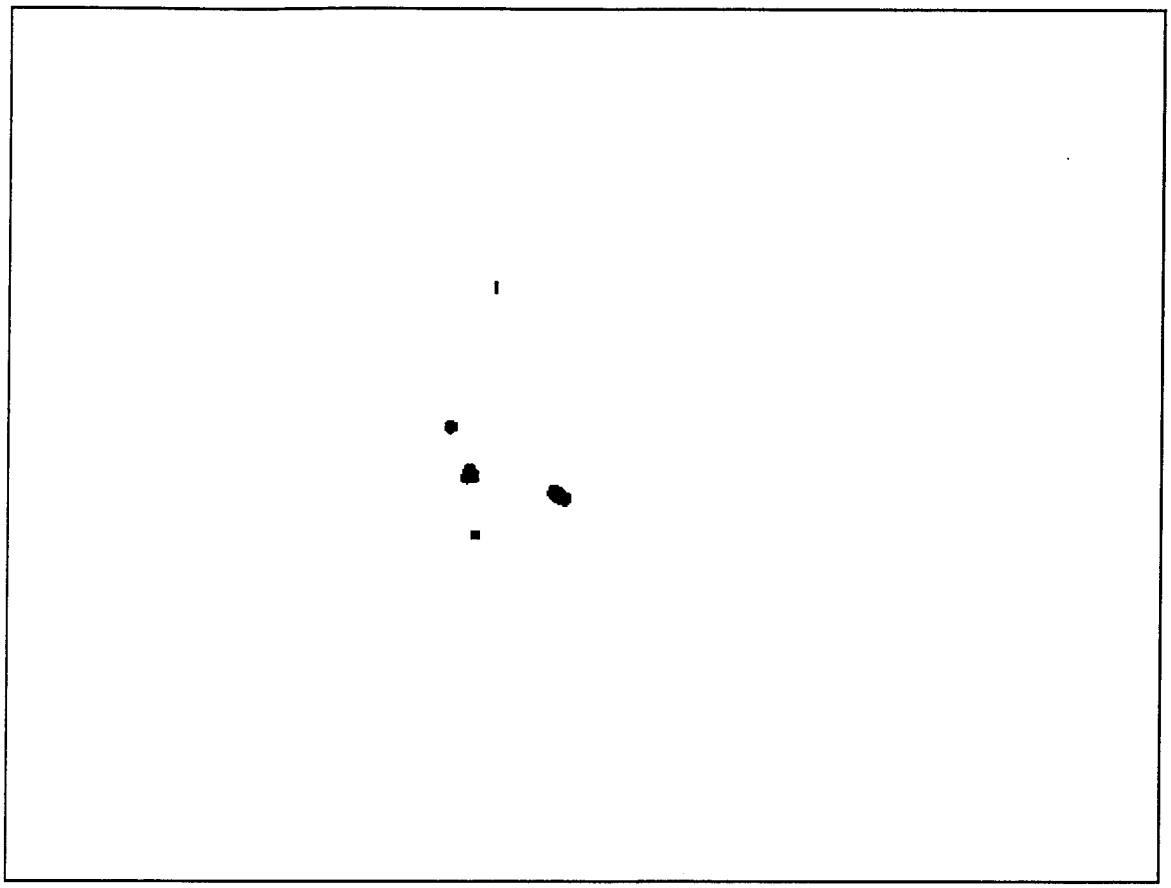

Figure M.3 - The same data as Figure M.1 but processed to show only the brightest flashes.

In conclusion, it should be mentioned that many optimizations are available for implementation in the prototype instrument. We will develop optics specifically for imaging a 1 mm field-of-view with special attention to the collection efficiency.

The lens will have to have the following characteristics:

(1) A field-of-view of 1 mm
(2) Optimized collection efficiency
(3) Capable of being mounted with the objective end in a high vacuum system

The prototype instrument will also use a fiber-optically coupled intensified CCD camera to improve the camera sensitivity.

Appendix N - Scintillator Output with Fission Fragments

Overview -

The goal of this experiment is to measure the light output from a ZnS(Ag) scintillator to determine:

(1) if fission fragments produce enough light to be measured with a CCD camera and
(2) if it is possible to use light output alone to distinguish between α-particle and fission fragments.

Natural uranium in the form U_3O_8 was used as a source of both α-particles and fission fragments. Unlike californium which spontaneously fissions, uranium must be induced to fission with thermal neutrons. Using uranium offers the benefit of being able to turn on/off the fission process by controlling the neutron flux. Otherwise the induced fission fragments from uranium are very similar in energy and mass to spontaneous fission fragments from californium[24]. The U_3O_8 in powder form was mounted between the scintillator material and a piece of 6 μm mylar film.

The apparatus is designed to be able to simultaneously measure the energy spectrum of the energetic ions and the light output from a scintillator struck by these ions. The light output is measured with a photomultiplier tube (PMT) and the particle energy is measured with a surface barrier detector. Figure N.1 shows a schematic overview of the apparatus configuration. The output from either the PMT or the surface barrier can be measured with the multi-channel analyzer by removing the linear gate.

Fission fragments can be distinguished from α-particles because of the following characteristics.

(1) Fission fragments produce a larger signal on the surface barrier than α-particles.

(2) Fission fragments occur in coincident pairs. If we only measure the PMT signal whenever a sufficiently energetic pulse has been measured on the surface barrier most of the spurious α-particle events can be eliminated.

The apparatus is divided into two modules. The U_3O_8 source and the detectors are mounted in proximity to a moderated neutron source. This apparatus is mounted in a water tight drum, which, along with a neutron source, is sunk in a larger drum filled with tap water. The water filled drum serves to moderate the energetic neutrons from the neutron source and to reduce the neutron exposure for the operating personnel. The neutron induced fission rate for uranium is orders-of-magnitude larger for thermal (moderated) neutrons than for energetic neutrons. The second module consists of the remainder of the equipment (amplifiers, computers, etc.) and is located away from the neutron source.

---

24 E. Segrè, *Nuclei and Particles*, 2nd ed. (Benjamin, New York, 1977)

H. Henschel *et al*, Nucl. Inst. and Meth. 190 (1981) 125-134

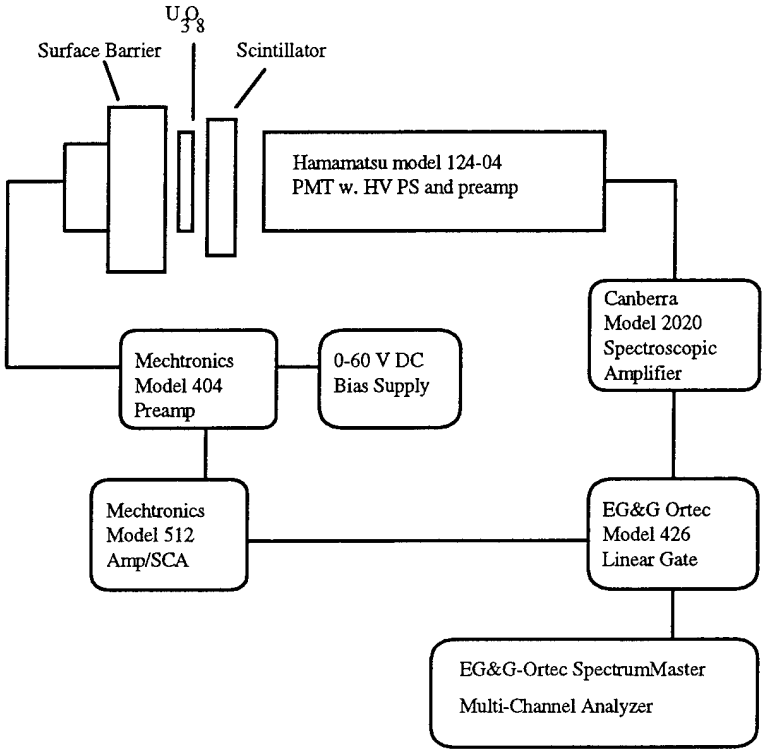

Figure N.1 - Schematic overview of the apparatus

Only the equipment which needs to be close to the U_3O_8 source is mounted in the water tight drum. The PMT, surface barrier, preamplifier, bias supply, a box to facilitate wiring and the U_3O_8 sample are mounted on 13" x 13" wooden board. The wooden board is attached perpendicular to the inside of the lid of an 8 gallon water tight steel drum with a pair of angle brackets. The board is positioned in 15" diameter drum so that the board slips into the center of the drum. Four lead bricks are mounted around the edge of the drum so as not to obstruct the apparatus board. Each lead brick weighed approximately 26 lbs. and together they weigh enough to sink the drum. The bricks are bolted to the walls of the drum with metal strapping tape so they can not shift. The necessary power cable and two 50 Ω coaxial signal cables are mounted through the lid of the drum. The hole is filled with black RTV to seal out water and light. All other holes

EG&G Ortec model 921 SpectrumMASTER
Mechtronics model 512 Amplifier and SCA
EG&G Ortec Model 426 Linear Gate
Tennelec Model TB3 NIM cage
EG&G Maestro II MCA emulator
100 MHz '486 AT-clone
Hamamatsu model 124-04 photomultiplier tube with HV-PS and preamp
60 V DC bias supply for surface barrier detector
Quantrad surface barrier detector
Canberra model 2020 spectroscopy amplifier
1 mCi neutron source in a water bath

Table N.1 - Apparatus

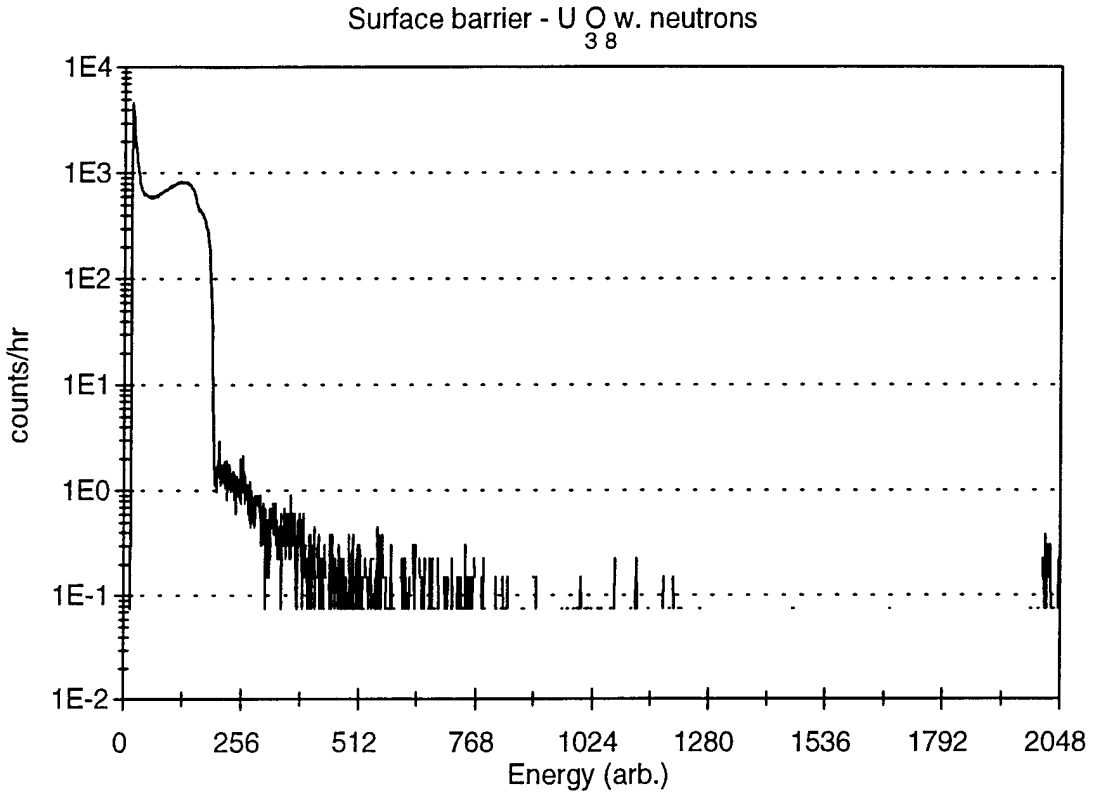

Figure N.2 - Plot showing an spectrum of particle energies measured with a surface barrier. The sample was U_3O_8 bathed in thermal neutrons. The counts at energy values above 2000 are unambiguously attributed to fission fragments.

in the drum are also sealed with RTV.

The scintillator/U_3O_8 source was constructed using the following procedure. A piece of ZnS(Ag) impregnated mylar was taped to a 2" diameter washer with the active side facing away from the washer. The active side of the scintillator was coated with a thin layer of Elmer's Spray Epoxy and U_3O_8 was sprinkled on the surface. The U_3O_8 was brushed over the surface to evenly cover the scintillator with an almost opaque layer of uranium oxide. The excess U_3O_8 is removed by turning the washer on its side and tapping the edge. A single layer of 6 μm mylar is stretched over the surface of the U_3O_8 covered scintillator. The same epoxy which holds the U_3O_8 to the surface also serves to glue the mylar to the washer. The edges of the washer are trimmed to remove excess scintillator material and mylar. A strip of adhesive tape is mounted around the edge of the washer to stop any U_3O_8 from escaping. Extensive precautions were observed to ensure that the U_3O_8 was contained and that the apparatus and personnel were not contaminated.

The mylar side of the scintillator/U_3O_8 source was mounted 3 mm from the surface of the surface barrier detector. The scintillator side of the source was mounted about 6 cm from the PMT photocathode.

The preamplified output of the PMT is amplified with a Canberra model 2020 spectroscopic amplifier. The amp serves both to amplify the PMT output and to shape the pulse

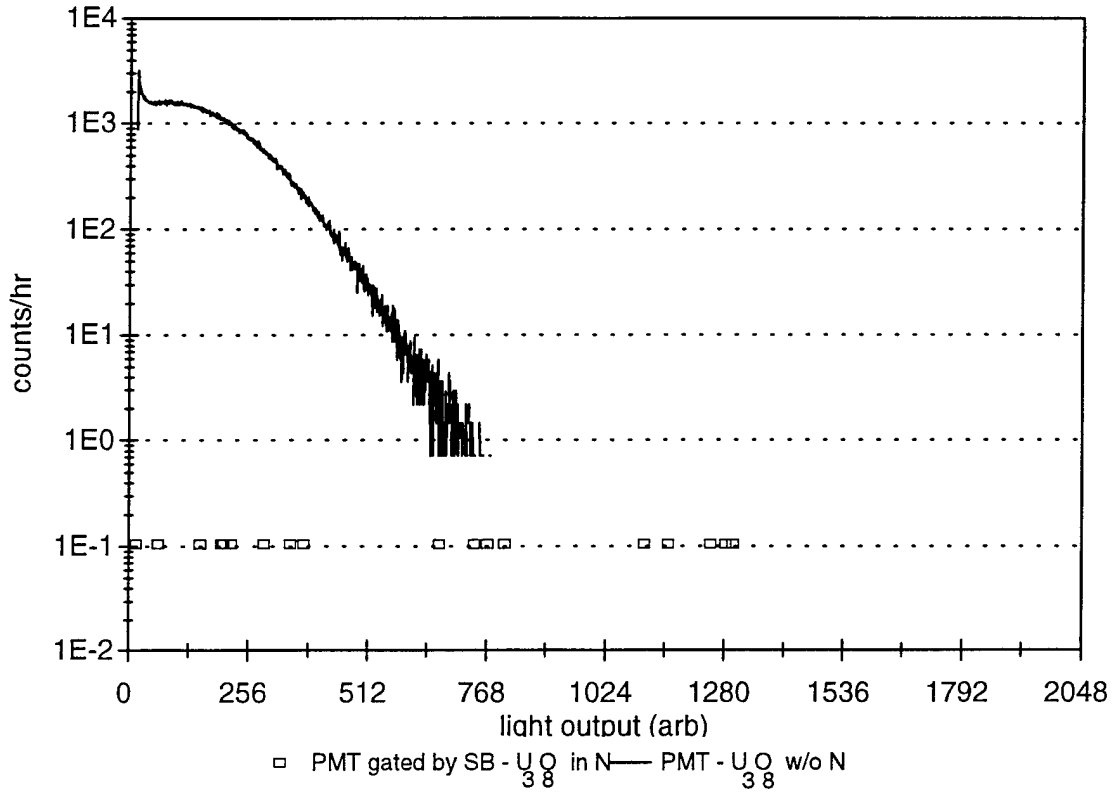

Figure N.3 - Light output spectrum for U_3O_8. The line shows the light output for α-particles. The boxes show the light output for the PMT gated with the surface barrier to exclude all events except fission fragments.

output with a 1 μs shaping time constant. When multiple pulses from the PMT occur during the 1 μs shaping time, the pulses are integrated together to give an increased output pulse height.

The surface barrier detector is a Quantrad model PP-450-100-18. It requires a bias voltage of 20 - 60 V DC which was provided by a battery powered bias supply. The output of the Quantrad is preamplified with a Mechtronics model 404 and amplified with a Mechtronics model 512 amplifier/single channel analyzer. The single channel analyzer feature of the model 512 is used to provide a gate pulse. Whenever the amplifier measures a sufficiently energetic particle, the SCA sub-section outputs a logic level pulse. The energy level can be set to an appropriate/interesting level and this pulse can be used to gate the PMT output.

A pulse height spectrum from either the surface barrier or the PMT was be recorded with a 2000 channel EG&G Ortec SpectrumMASTER multi-channel analyzer.

Results -

Among the first things we needed to demonstrate was that we were in fact able to produce and measure fission fragments. Since the α-particles will have energies of less than 5 MeV and the fission fragments could be as energetic as 100 MeV, the surface barrier detector gives the clearest

signature of fission fragments. Figure N.2 shows surface barrier data which clearly demonstrates that we were able to see fission fragments. The horizontal axis is signal size and the vertical axis is the number of counts per hour. The horizontal axis is not calibrated but should be within 20% of linear with respect to particle kinetic energy. We attribute the large number of counts at smaller kinetic energies (0-200) due primarily to α-particles. We verified this conclusion by comparing this data with data from the same source without neutrons and an ^{241}Am α-particle source. The counts above 2000 are much more energetic than any events seen with a pure α-particle source and thus are attributed to fission fragments. The data in the range between 200 and 2000 is less clear cut. It is due to a combination of α-particles and fission fragments.

With this information, we know where to set a gate so as to exclude almost all α-particles by surface barrier signal size alone. Of course, we have the additional characteristic of fission fragment events, the simultaneity of the surface barrier and the scintillation events, to assist in eliminating all false signals. We thus chose only to measure the PMT when the surface barrier had simultaneously recorded a event with energy greater than channel 281. By simultaneous we mean that when the faster amplifier on the surface barrier measures a sufficiently energetic particle, the gate opens for 4 μs to measure pulses on the PMT.

Figure N.3 shows scintillator light output as measured by the PMT. The horizontal axis is linear in light output and the vertical axis counts the number of pulses of each energy per hour. The data plotted as a line is the characteristic light output of the ZnS(Ag) scintillator struck with α-particles. This data was recorded in 5000 seconds. The data points shown as boxes in figure N.3 shows data in which the PMT is gated by the surface barrier set to exclude α-particles. We attribute each of these points to fission fragments. Each box represents one count and during 13 hrs. 20 mins. (48,000 secs.) of acquisition we recorded 19 events.

Interpretation of this data is not entirely straight forward. The light output from the events attributed to fission fragments range from values typical of α-particles to larger than typical for α-particles. The five events above 1024 clearly show that some of the fission fragment events produce more light output than all the α-particles. The remainder of the events are more troublesome given our initial goals because it would be impossible to distinguish them from α-particles by light output alone. This may be due to an artifact of the experiment. The U_3O_8 source we used in this experiment was optimized to produce the largest number of fission fragments by making the U_3O_8 layer thicker. The unfortunate result of this optimization is that the fission fragments tend to loose much of their energy before they escape the source. This is particularly evident if we consider the current experimental configuration. Those fission events which occur closest to the surface barrier are most likely to trigger the gate. However, these events must pass through the most material to escape the other side of the source and activate the scintillator. This *may* explain some or all of the lower intensity light outputs we measured.

To improve on this data, we constructed a new U_3O_8 source which had a significantly thinner layer of U_3O_8. We expect the rate of fission events would be slower but that each event would loose less energy and would be measured more accurately. Our attempts to repeat this experiment with the new source were frustrated when the Mechtronics model 512 amp/SCA broke. We tried unsuccessfully to replace the SCA with an alternative from Greenspan, Inc.

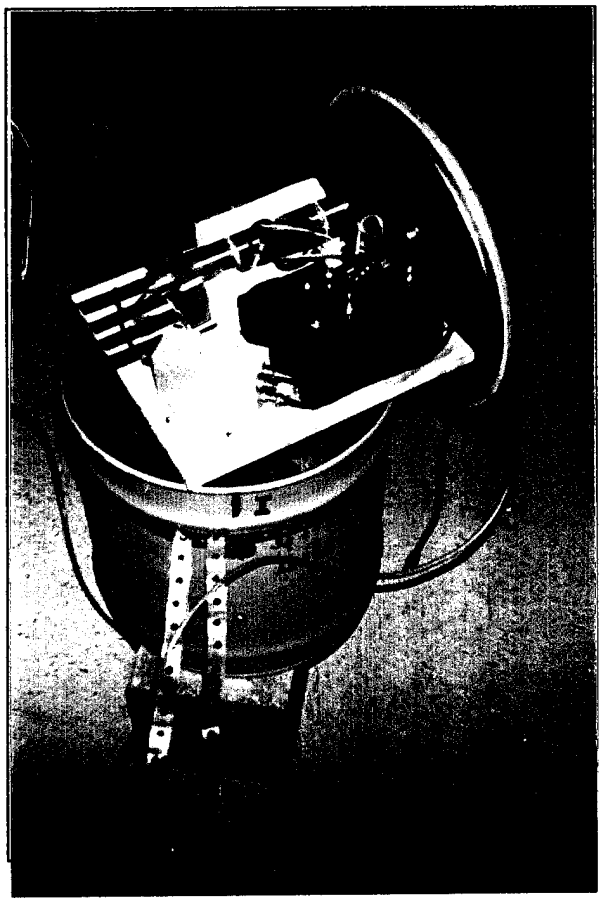

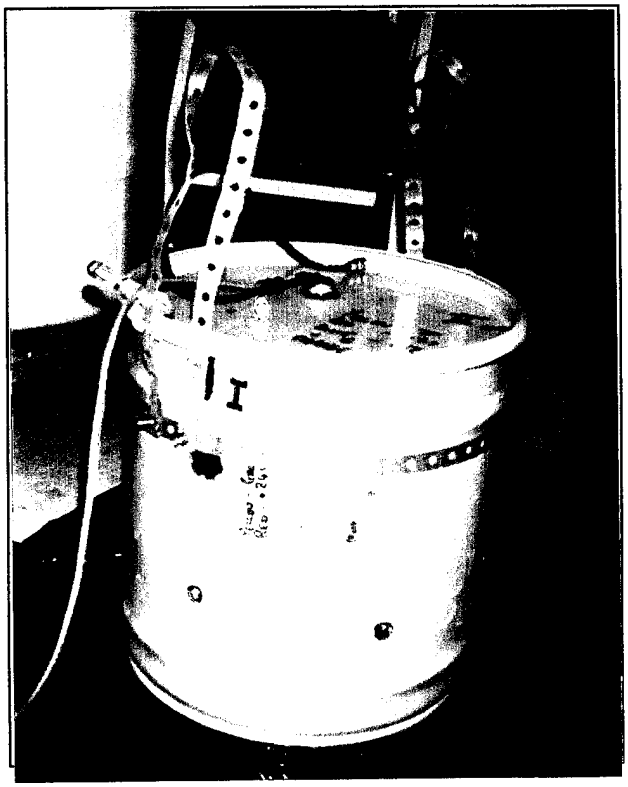

Photographs of the apparatus for the experiment performed in Houston at Greenspan, Inc. The experiment tested the light output from a ZnS(Ag) scintillator due to α-particles and fission fragments.

Left - Surface barrier and photo-multiplier tube and associated electronics as mounted inside the drum.

Below - A barrel of water containing the neutron source and electronic drum. Also shows the NIM bin of amplifers and the multichannel analyzer.

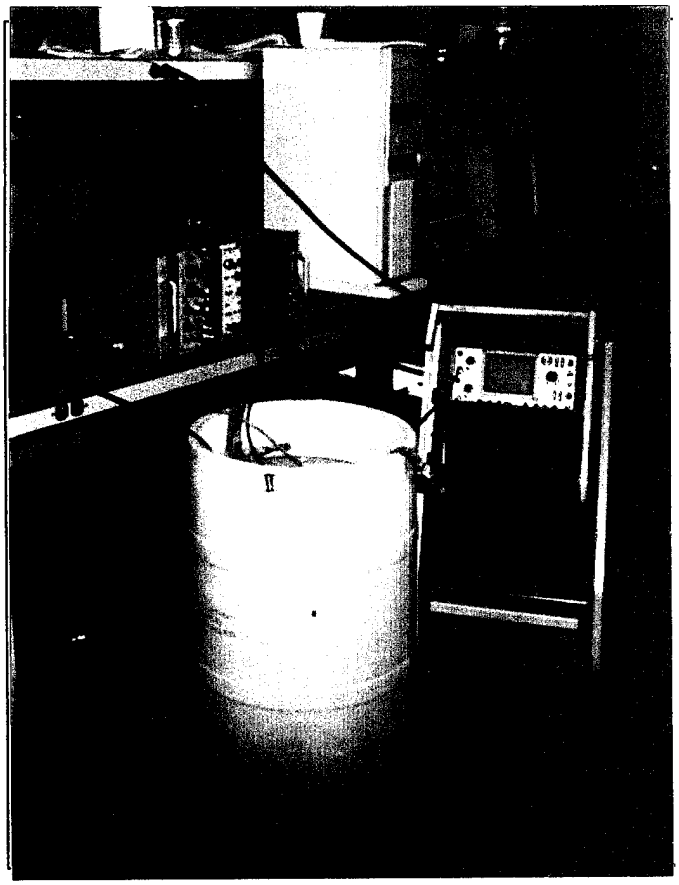

Left - The water-tight drum containing the PMT and surface barrier.

Conclusions -

From this investigation we demonstrate that some (~1/4) of the fission fragments produce more light than all the α-particles. It may be that much more than 1/4 of the fission fragments produce more light than all the α-particles but due to equipment difficulties we are not able to show this.

The result of this experiment is sufficient to demonstrate the feasibility of distinguishing some fission fragments from α-particles using image intensity data alone. A system which would trigger only when a sufficiently bright scintillation occurred might miss a significant fraction of the total fission fragment events. However such a system would not mistakenly identify α-particles as fission fragments.

We expect to repeat this experiment when the apparatus is repaired. We probably would use a Cf source to increase the number of fission fragments and thus decrease the amount of time necessary to collect statistically significant data.

Appendix O - X-ray test

In the Phase I proposal we had proposed testing whether fission fragments would produce a detectable large quantity of x-rays when they struck the sample. The x-ray spectrum of a material is an excellent way to do elemental identification. Each element has a characteristic x-ray spectrum and even in samples containing many elements it is often possible to determine the elemental composition from an x-ray spectrum. This technique is common in scanning electron microscopes where a beam of 20-30 keV electrons knock inner shell electrons from their orbitals. The recombination process is accompanied by the release of x-rays.

Part of the proposal had included limited bench level tests to determine whether fission fragments would produce x-rays when they struck samples. As we did not have access to a fission fragment source we decided to experiment with α–particles. Hank Lentz and I tested an aluminum sample and a copper-beryllium sample in the RJ Lee Instruments, Ltd.'s PersonalSEM. We used a Po source as a source of 5 MeV α–particles. The integral x-ray detector in the PersonalSEM was used to record x-ray emission from the samples. In both samples, clear Al peak was evident. (The Al peak with the Cu-Be sample can be attributed to the Al stage.) The spectrum developed a couple orders of magnitude slower than for an electron beam. This is probably due to the lower flux of α–particles. There was less evidence for the development of a Cu spectrum. It was developing but it developed a couple orders of magnitude slower than even the Al spectrum. It was interesting that only the lower energy peaks were evident. This may evidence that α–particles interact with decreasing frequency with electrons as they become more tightly bound.